

# Multi-millennial human impacts and climate change during the Maya early Anthropocene: implications on hydro-sedimentary dynamics and socio-environmental trajectories (Naachtun, Guatemala)

Cyril Castanet, Louise Purdue, Marc Testé, Aline Garnier, Anne-Lise Develle-Vincent, Fatima Mokadem, Christine Hatté, Caroline Gauthier, Philippe Lanos, Philippe Dufresne, et al.

# ▶ To cite this version:

Cyril Castanet, Louise Purdue, Marc Testé, Aline Garnier, Anne-Lise Develle-Vincent, et al.. Multimillennial human impacts and climate change during the Maya early Anthropocene: implications on hydro-sedimentary dynamics and socio-environmental trajectories (Naachtun, Guatemala). Quaternary Science Reviews, 2022, 283, pp.107458. 10.1016/j.quascirev.2022.107458. hal-03628387

# HAL Id: hal-03628387 https://hal.science/hal-03628387v1

Submitted on 22 Jul 2024

HAL is a multi-disciplinary open access archive for the deposit and dissemination of scientific research documents, whether they are published or not. The documents may come from teaching and research institutions in France or abroad, or from public or private research centers. L'archive ouverte pluridisciplinaire **HAL**, est destinée au dépôt et à la diffusion de documents scientifiques de niveau recherche, publiés ou non, émanant des établissements d'enseignement et de recherche français ou étrangers, des laboratoires publics ou privés.

Copyright

# Multi-millennial human impacts and climate change during the Maya early Anthropocene: implications on hydro-sedimentary dynamics and socio-environmental trajectories

# (Naachtun, Guatemala).

# Authors names

- Cyril Castanet<sup>1</sup>
- Louise Purdue<sup>2</sup>
- Marc Testé<sup>3</sup>
- Aline Garnier<sup>4</sup>
- Anne-Lise Develle-Vincent<sup>5</sup>
- Fatima Mokadem<sup>6</sup>
- Christine Hatté<sup>7</sup>
- Caroline Gauthier<sup>8</sup>
- Philippe Lanos<sup>9</sup>
- Philippe Dufresne<sup>10</sup>
- Eva Lemonnier<sup>11</sup>
- Lydie Dussol<sup>12</sup>
- Julien Hiquet<sup>13</sup>
- Philippe Nondédéo<sup>14</sup>

# Authors affiliations

- <sup>1</sup> Université Paris 8 Vincennes Saint-Denis, Laboratoire de Géographie Physique, Environnements quaternaires et actuels (LGP UMR CNRS 8591), 2 rue de la Liberté 93200 Saint-Denis, France. cyril.castanet@lgp.cnrs.fr Corresponding author.
- <sup>2</sup> Université Côte d'Azur, Laboratoire Cultures et Environnements. Préhistoire, Antiquité, Moyen Âge, CEPAM UMR CNRS 7264, Pôle Universitaire Saint Jean d'Angély, SJA 3, 24, avenue des Diables Bleus, F 06300 Nice, France. louise.purdue@cepam.cnrs.fr
- <sup>3</sup> Laboratoire de Géographie Physique, environnements quaternaires et actuels, LGP UMR CNRS 8591, 1, Place Aristide Briand, 92195, F – Meudon, France marc.teste@lgp.cnrs.fr
- <sup>4</sup> Université Paris-Est Créteil, UPEC, Laboratoire de Géographie Physique, environnements quaternaires et actuels, LGP UMR CNRS 8591, 1, Place Aristide Briand, F 92195 Meudon, France. aline.garnier@lgp.cnrs.fr

- <sup>5</sup> Laboratoire Environnements, DYnamiques et TErritoires de la Montagne, EDYTEM UMR CNRS 5204, Université Savoie Mont Blanc, Bâtiment « Pôle Montagne », 5, bd de la mer Caspienne, F 73376 Le Bourget du Lac, France. anne-lise.develle@univ-smb.fr
- <sup>6</sup> Laboratoire de Géographie Physique, environnements quaternaires et actuels, LGP UMR CNRS 8591, 1, Place Aristide Briand, 92195, F Meudon, France fatima.mokadem@lgp.cnrs.fr
- <sup>7</sup> Laboratoire des Sciences du Climat et de l'Environnement, LSCE UMR 8212 CEA, CNRS, UVSQ, Université Paris-Saclay, CEA Saclay, Bat 714, Site de l'Orme des Merisiers, Chemin de Saint Aubin RD 128, F-91191 Gif sur Yvette, France. christine.hatte@lsce.ipsl.fr
- <sup>8</sup> Laboratoire des Sciences du Climat et de l'Environnement, LSCE UMR 8212 CEA, CNRS, UVSQ, Université Paris-Saclay, CEA Saclay, Bat 714, Site de l'Orme des Merisiers, Chemin de Saint Aubin RD 128, F-91191 Gif sur Yvette, France caroline.gauthier@lsce.ipsl.fr
- <sup>9</sup> CNRS, UMR 5060 IRAMAT-CRP2A, Université Bordeaux Montaigne et UMR 6118 Géosciences-Rennes, Université de Rennes 1, France philippe.lanos@univ-rennes1.fr
- <sup>10</sup> CNRS, UMR 5060 IRAMAT-CRP2A, Université Bordeaux Montaigne et UMR 6118 Géosciences-Rennes, Université de Rennes 1, France philippe.dufresne@univ-rennes1.fr
- <sup>11</sup> Université Paris 1 Panthéon Sorbonne, Laboratoire Archéologie des Amériques, ARCHAM UMR CNRS 8096, Centre Malher, 9 rue Malher, F-75004 Paris, France. eva.lemonnier@univ-paris1.fr
- <sup>12</sup> Université Côte d'Azur, Laboratoire Cultures et Environnements. Préhistoire, Antiquité, Moyen Âge, CEPAM UMR CNRS 7264, Pôle Universitaire Saint Jean d'Angély, SJA 3, 24, avenue des Diables Bleus, F 06300 Nice, France. lydie.dussol@cepam.cnrs.fr
- <sup>13</sup> Laboratoire Archéologie des Amériques, ARCHAM UMR CNRS 8096, Centre Malher, 9 rue Malher, F-75004 Paris, France. julien.hiquet@hotmail.fr
- <sup>14</sup> Laboratoire Archéologie des Amériques, ARCHAM UMR CNRS 8096, Centre Malher, 9 rue Malher, F-75004 Paris, France. philippe\_nondedeo@yahoo.com

# Corresponding author

Cyril Castanet

Université Paris 8 Vincennes Saint-Denis, Laboratoire de Géographie Physique, Environnements quaternaires et actuels (LGP UMR CNRS 8591), 1, Place Aristide Briand, F – 92195 Meudon, France. cyril.castanet@lgp.cnrs.fr

#### 1

2

3

4

5

6

7

8

9

10

11

12

13

14

15

16

17

18

19

20

21

22

23

24

25

26

#### **Abstract**

During the Maya early Anthropocene (2000 BCE - 1000 CE) in Mesoamerica, socio-environmental interactions contributed to the rise and decline of the ancient Maya civilisation. At the scale of the exploitation territories of the Maya cities, the temporal variations of hydrological and sedimentary dynamics in response to anthropogenic and climate drivers are still poorly known. This constrains diachronic analyses of socio-ecosystems and, more particularly, of water and soil resources in the hinterlands. This manuscript analyses and presents a regional comparison of the dynamics of one of the most transformed hydrosystems and morpho-sedimentary systems by the societies of the Southern Maya Lowlands (SMLs), during the second half of the Holocene. It focuses on the lake basin of the polje named El Infierno bajo and its watershed, which was the main water storage area for the Maya city of Naachtun – a large regional capital between 150 and 950 CE –, and which contains many remains of hydraulic and agrarian structures. This integrated palaeolimnological, geoarchaeological and hydrological approach, based on the analyses of morpho-sedimentary archives, LiDAR altimetry data and hydrological data, resulted in the construction of hydro-sedimentary baselines (pre-synand post- ancient Maya anthropogenic impacts). Currently, the intermittent lake (civale) of this bajo responds to strong seasonal and interannual hydrological variabilities, under climate control. During the past 5500 years, hydro-sedimentary fluctuations were marked by the alternation of seven main hydrological periods (HP), characterised by high and low lake levels (alternately perennial, intermittent and dry lake) and six main erosion and sediment transfer periods (ESTP), marked by strong and low alluvial and colluvial detrital inputs in the lowlands. Anthropogenic and climate forcings have independently or jointly controlled the hydrologic and sedimentary budgets of the lake basin. Lithofacies, depositional processes, accumulation rates and drivers of the anthropogenic detrital inputs – the so-called "Maya clays" –, are analysed and quantified from ~1500 BCE to ~1150 CE. It thus reveals one of the longest periods of occupation and exploitation of natural resources of the SMLs, for over 2500 years during the Preclassic, Classic and Post-classic Maya periods. The hydrosedimentary dynamics in the *bajos* of the SMLs Elevated Interior Region (EIR), such as El Infierno, enabled the long-term exploitation of water and soil resources for agrarian purposes, thanks to the construction of hydraulic and agrarian palimpsest landscapes shaped by the socio-ecosystems.

# Keywords

- 31 Anthropocene, Palaeolimnology, Geoarchaeology, Sedimentology (lakes & swamps), Central
- 32 America, Wetland, Polje, *Bajo*, Anthropization, Erosion, Maya, Naachtun

33

34

35

36

37

38

39

40

41

42

43

44

45

46

47

48

49

50

27

28

29

30

# 1. Introduction

In the current context of global changes (climatic, environmental and societal), knowledge of the long-term dynamics of water and soil resources in response to anthropization and climate change is a major ecological and societal challenge (Padrón et al. 2020; Roberts et al. 2017; Stephens et al. 2019; Veldkamp et al. 2020). In the Mesoamerican tropics, research on the processes controlling the rise and decline of Maya civilization regularly questions the importance of socio-environmental interactions related to resource exploitation and/or climate change (Aimers 2007; Douglas et al. 2015, 2016; Hodell et al. 1995; Kennett et al. 2012; Turner and Sabloff 2012). Ancient Maya impacts on the Earth's surface between 2000 BCE and 1000 CE represent an early Anthropocene analog (Beach et al. 2015; Kennett and Beach 2013). Recently, large-scale work in the SMLs has renewed our knowledge of the complexity of ancient Maya land use (Canuto et al. 2018). The SMLs appear to be one of the most densely populated regions in the world for its time (7 to 11 million inhabitants at the height of the Late Classic period, 650 to 800 CE). Some ancient territories, such as those of the cities of Tikal and Naachtun, appear to have been densely populated and developed to ensure the subsistence of populations through water and soil management. For all archaeological periods combined, the Naachtun exploitation territory presents the highest density of archaeological structures (89 str./km²) and the highest density of hydraulic and agrarian structures in seasonal marshes (*bajos*) (22.5% of the territory) of all the studied territories, covering more than 2000 km² (Canuto et al. 2018; Castanet et al. 2019; Nondédéo et al. in press).

53

54

55

56

57

58

59

60

61

62

63

64

65

66

67

68

51

52

The dynamics of water and soil resources in the SMLs have evolved in response to biophysical environments, social demand and climate (Dunning et al. 2002). The Elevated Interior Region (EIR) is at the heart of the geographic area in which the ancient Maya civilization of the SMLs evolved (Dunning et al. 2012). Karst depressions – or poljes – locally known as bajos account for up to half of the ancient Maya territories (Pope and Dahlin 1989; Siemens 1978). Nowadays in these karst depressions, perennial or intermittent water bodies locally named civales are the only wetlands and water sources in the EIR (Dunning et al. 2002; Lundell 1937). The presence of perennial lakes within the bajos during the Preclassic and/or Classic Maya periods has been debated, with some authors arguing that they were absent (Cowgill and Hutchinson 1963) and others that they were present (Cooke 1931; Dunning et al. 2002; Ricketson 1937). The agricultural use of bajos has also been debated, with some authors pointing to unfavourable edaphic conditions for crops (Dahlin and Dahlin 1994; Pope and Dahlin 1989, 1993) and others to favourable conditions (Beach et al. 2003; Culbert et al. 1996; Culbert et al. 1989; Dunning et al. 2002; Kunen et al. 2000; Palerm and Wolf 1957; Turner and Harrison 1983). Knowledge of the hydro-sedimentary and socio-environmental dynamics in the bajos is therefore crucial for understanding the history of interactions between the ancient Maya, their environment and climate.

70

71

72

73

74

75

76

69

Work over the last three decades has established that in the Late Holocene (Preclassic and Classic Maya periods, see Fig. 11), the *bajos* and *civales* experienced hydrological and sedimentary dynamics with fluctuations controlled by anthropogenic and climate drivers (Beach et al. 2003, 2008, 2018; Dunning et al. 2002, 2019; Dunning and Beach 1994; Wahl et al. 2006, 2013, 2014, 2016). Their infilling with detrital inputs in response to Maya anthropogenic impacts (Maya clays) modified their hydrological dynamics (Beach et al. 2003; Dunning et al. 2002). The study of the sedimentary records

of these environments is frequently complicated by palustrine lithofacies, limited thickness and discontinuous layers. In addition, these records are frequently pedogenised and deformed by argilliturbation (Beach et al. 2003; Dunning et al. 2002). These facts constrain reconstructions. In addition, some methodological and analytical developments would allow for a better understanding of the hydro-sedimentary dynamics of the *bajos* lake basins. On the one hand, this involves palaeohydrological (water volumes and surfaces) and sedimentological (fluxes of mineral phases of the deposit) quantifications (Wahl et al. 2016). On the other hand, it requires to take into account current hydrological dynamics.

This study implements a multi-scalar and integrated palaeolimnological, geoarchaeological and hydrological approach to the lake basin of the main *bajo* of Naachtun hinterland. Based on the characterisation, both on the field and in laboratory, of sedimentary records, on LiDAR altimetric and on hydrological data, our study aims to overcome the limits described above in order to examine the following two questions. In one of the most densely populated hinterlands of the Maya early Anthropocene, what were the hydrological and sedimentological responses to anthropogenic and climate changes? How past hydro-sedimentary dynamics shed light on the history of anthropization and of water and soil resources availability of the ancient Maya?

#### 2. Regional settings

2.1 Geomorphological, hydrological, climatic and biogeographical contexts.

The study area is located in the southern Yucatan Peninsula in the Maya Biosphere Reserve of Guatemala, and includes the Classic Maya site of Naachtun and part of its exploitation territory. It lies between 260 and 330 m a.s.l. in the Elevated Interior Region (EIR) of the SMLs (Fig. 1). The karstified limestone plateaus are developed on Tertiary (Palaeocene, Eocene) carbonate sedimentary beds (Instituto Geographico Nacional 1970; Perry et al. 2019; Servicio Geológico Mexicano 2007; Vinson

1962). The karst landform is dominated by alternating hilly and flat low-lying areas. The latter are poljes (*bajos*), valleys and sinkholes. North of the centre of Naachtun are the *bajo* El Infierno and three *civales*, aligned along a tectonic structural direction, relative to the phases of tectonic uplift of the Peninsula (Fig. 1) (Lugo-Hubp et al. 1992; Lugo-Hubp and Garcia 1999; Padilla 2007; Perry et al. 2009). The Quaternary superficial deposits and soil cover are contrasted. The shallow, drained soils of the hills (Mollisols, Inceptisols, Alfisols) alternate with the heavy, thick soils of the *bajos* (Vertisols, Histosols) (Bautista et al. 2011; Beach et al. 2018; Dunning et al. 2019; Simmons et al. 1959). Karst depressions are the main storage areas for detrital inputs, particularly the Maya clays that result from anthropogenic forcing of denudation (Beach et al. 2003; Deevey et al 1979; Dunning et al. 2002).

The high porosity of the rock, the great aquifer depth and the current climate induce low limnicity in the EIR. Rivers and lakes are scarce and often intermittent (Beach et al. 2009; Deevey et al. 1979; Dunning et al. 2012). The El Infierno *bajo* includes a closed lake depression with a surface area of 1.13 km², of karstic origin (Fig. 1). It currently includes a wetland structured around three *civales*, which distinguishes this *bajo* from the majority of others (Castanet et al. 2016). Its catchment has a surface area of 17.3 km², the eastern boundary of which corresponds to the watershed between the hydrosystem of the Rio Candelaria, which flows into the Gulf of Mexico, and that of the Rio Azul, which flows into the Rio Hondo and the Caribbean Sea. Water and sediment inputs into this closed basin occur through intermittent tributaries (T1 to T5, Fig. 1), slopes directly connected to the depression (surface run-off) and ground water run-off. Water is released by evapotranspiration (ETP), infiltration and flow through ponors or swallow holes. Under theoretical overflow conditions, lake outflow occurs towards the north, at a basin mouth located at 268.4 m a.s.l. (Fig. 1).

The climate controlling water inputs to this hydrosystem is warm sub-humid, type Aw according to the modified Köppen classification (García 1981, 1990). The precipitation regime of the Petén shows

an annual average rainfall of 1600 mm and significant interannual variability (900 to 2500 mm / year) (Deevey 1978; Rosenmeier et al. 2002a). A dry season with only 10% of annual precipitations (from January to the end of May) alternates with a rainy season, interspersed in July-August with the midsummer brief dryer period (García 1990; Magaña et al. 1999; Small et al. 2007). These dynamics are controlled by the mobility of the InterTropical Convergence Zone (ITCZ) and more broadly by the interactions of the tropical Atlantic and Pacific Oceans (Enfield and Alfaro 1999; Giannini et al. 2000; Taylor et al. 2002, 2011). Climatic variability in the Maya area during the Holocene was punctuated by relatively drier periods, particularly during the Late Holocene (Curtis et al. 1996; Douglas et al. 2015, 2016; Haug et al. 2001; Hodell et al. 2005a; Kennett et al. 2012; Medina-Elizalde et al. 2010; Rosenmeier et al. 2002a; Wahl et al. 2013, 2014, 2016). A number of factors that controlled Late Holocene hydroclimate in the area have been proposed, such as solar variability, North Atlantic climate variability, shifts in the position of the Intertropical Convergence Zone, Pacific Ocean influences (ENSO) and Interoceanic temperature gradients. There is no consensus among researchers regarding a single causal mechanism (Douglas et al. 2016).

The watershed of this lake basin is currently covered by the semi-evergreen tropical forest typical of Northern Petén (Lundell 1937). The *civales* and the margins of the *bajo* currently display four plant community types distributed according to gradients in soil moisture and/or seasonal flooding. The hill zone comprises two other plant community types (Testé et al. 2020).

#### 2.2 Archaeological context

Naachtun was a large regional capital during the Classic period (150 - 950 CE), and the centre of the Maya city was located near the *bajo* and its lake basin (Figs 1D and 1E). The earliest archaeological remains found in the Naachtun hinterland date back to the Middle Preclassic period to ~ 600 BCE. Several preclassic centres of power have been identified here. They were influenced by the development of monumental cities, such as the capitals of El Mirador and Nakbe, built during the

Middle and Late Preclassic, ~18 km southwest of the study area. These cities were abandoned around 150 CE (Hansen 1990; Wahl et al. 2007). During the Classic period, Naachtun experienced a first political climax in the Early Classic (300-450 CE), related to Teotihuacan's control of the SMLs, and a second, demographic peak during the Late and Terminal Classic (750-950 CE) (Nondédéo et al. in press; Nondédéo et al. 2019). Subsequently, Naachtun did not escape the crises affecting the SMLs until the Terminal Classic, as the city was abandoned around 950/1000 CE (Dussol et al. 2019; Nondédéo et al. in press). The population of Naachtun centre has been estimated to be between 580 and 1050 inhabitants around 300 CE, between 1100 and 1300 inhabitants around 550 CE and reached a maximum of approximately 2500 inhabitants during the second half of the Late Classic (750-830 CE) (Hiquet 2020). The population of Naachtun territory (in the 135 km² surveyed area) was estimated to be at a maximum of 15,000 inhabitants around 300 CE (Hiquet 2020) and between 30,000 to 40,000 inhabitants around 750-830 CE (Canuto et al. 2018; Hiquet 2020). In the studied watershed, land-use remains are dated to the Preclassic and Classic periods up to ~ 950 CE (Figs. 1D and 1E). These are hydraulic and agrarian facilities (Castanet et al. 2019), but they also include numerous residential compounds as well as the construction of public, religious and political spaces (Nondédéo et al. in press).

170

171

172

154

155

156

157

158

159

160

161

162

163

164

165

166

167

168

169

**Fig. 1**. Maps of the El Infierno lake basin and its watershed within the Southern Maya Lowlands and the Elevated Interior Region: geomorphological, hydrological, geoarchaeological and archaeological aspects.

173

174

175

176

#### 3. Material and methods

Our methodological approach is based on six complementary methodological components, allowing the integrated study of the hydro-sedimentary dynamics of the lake basin and its watershed.

177

#### 3.1 Creation of a baseline of current hydrological dynamics

#### 3.1.1 Topographic and hydrographic modelling

The watershed, the potential intermittent drainage network and the lake depression of the *bajo* were modelled using a LiDAR Digital Elevation Model (DEM) and a Geographic Information System (GIS, Arcgis 10.6, Esri) (Figs 1D and 1E). LiDAR acquisition was produced by the National Center for Airborne Laser Mapping, as part of the Pacunam LiDAR Initiative (Canuto et al. 2018; Fernandez-Diaz et al. 2016). The DEM of the *bajo* has a resolution of 1 m and an accuracy of +/- 15 cm. Its systematic analysis was aimed at detecting karst landform features (such as drainage funnels, swallow holes, ponors, avens sinkholes), which were verified on the field.

#### 3.1.2 Hydrological measurements (piezometric probes), studies of the lichen trimline and of high-

#### water marks

The characterisation of the current seasonal and interannual hydrological fluctuations of the *civales* was based on two complementary methods. The first consisted of installing two observation wells (piezometric probes) in two *civales* (PP1 and PP2, Fig. 1E). The probes measured the cumulative hydrostatic and atmospheric pressures as well as the water temperature at a frequency of one measurement every 45 minutes, during the periods April 2015 - April 2019 (PP1) and April 2015 - April 2016 (PP2). A barometric correction was made using data acquired by a barothermal probe installed in the study area. The measured stages were repositioned in relation to the mean sea level (a.s.l.), thanks to positioning using LiDAR DEM. The second method is based on finding and estimating the height of two stage indicators of actual high water, located in the lake depression: high watermarks and Corticolous Crustose Lichen Trimline (CCLT) of the *bajo* trees (Hale 1984; Rosentreter 1992; Timoney and Marsh 2004). A batch of 16 CCLT observation stations were located within the *bajo* (seven inside and nine outside the lake depression) (Fig. 1E). Each station consisted of a living tree older than 15 years (age estimated by counting tree rings), with an upright trunk and bark colonised by a population of corticolous crustose lichens. Each station was geo-referenced using a handheld GPS. In the field, the relative elevation of each CCLT (where present) was measured

manually. The altitude a.s.l. of the CCLT was estimated secondarily using LiDAR DEM. The hydrography and estimated water surfaces and volumes, for the current seasonal high-water levels, were modelled in GIS, using the knowledge of the measured stages and the LiDAR DEM.

# 3.2 Characterisation of the stratigraphy of alluvial and colluvial records

The stratigraphy of the sedimentary fill of the lake depression was established through 49 sediment boreholes spaced on average 30 m apart and distributed along two transects crossing the entire depression (CS1 and CS2, Figs 1D and 1E). A hand auger was used allowing a vertical accuracy of 10 cm. Five cross sections were also excavated at the edge of the depression (including sections CS1-S2C, CS1-M1TER1 and CS2-S10). A core drilling was made in the central part of the depression (CS2-S1), using a hand gouge auger (Fig. 1E). Interpolations between the sedimentary borings were made by the lateral correlation of sedimentary lithofacies. This enabled two reconstructed stratigraphic section models (CS1 and CS2) to be proposed (Figs 1, 3, 4).

# 3.3 Sedimentological, pedological, geochemical and isotopic studies

The study is based on the analysis of three sediment series, CS1-S2C, CS2-S1 and CS2-S10 (Figs 1, 3, 4, 6, 7, 8). It includes several indicators of environmental change. The grain size of the deposits was interpreted using the percentage of grain size fractions and the D50 diameter of each sample grain-size distribution. The latter was measured by laser diffraction with a Beckman-Coulter LS230, after the destruction of organic matter (OM). Grain-size data allows us to interpret the energy of the depositional environment (e.g. the lutites, in § 4.3.1.1) but also of the fraction of carbonate authigenic minerals (e.g. the silt fraction, in § 4.3.1.2).

In order to characterise sediment composition, we measured the amount of total carbon/total sediment (TC) and the amount of organic carbon/leached sediment. The mass % of CaCO<sub>3</sub>/raw sediment was estimated assuming all inorganic carbon was bound in CaCO<sub>3</sub> (Appendix A). The content (%) of alumino-silicates and oxyhydroxides was estimated by subtracting the percentage of CaCO<sub>3</sub> and OM from 100%. The petrographic characterisation of the sediments of certain sediment

zones was carried out by making and studying thin sections of the sediment with a stereomicroscope, as well as by observing fraction particles greater than 25 microns.

229

230

231

232

233

234

235

236

237

238

239

240

241

242

243

244

245

246

247

248

249

250

251

252

253

254

The relative contents of elements were analysed using X-ray fluorescence (XRF) on the surface of the sediment core with an Avaatech Core Scanner. The relative contents (counts<sup>-1</sup>) of major elements (Si, Ca, Al, Fe, Ti, K, Mn, S, ...) and of heavier elements (Sr, Rb, Zr, Br, Pb, ...) were statistically analysed (Principal Component Analysis). In lacustrine and palustrine sediments, the nature and the ratio of the fractions of authigenic carbonated minerals (of biogenic and physicochemical origins) and of terrigenous detrital allochthonous minerals (silicate and carbonate minerals, oxides, ...) may result from several factors, such as erosion of watershed soil and rocks, fluctuation of lake level and of biophysical-chemical conditions of lake waters (Campy and Meybeck 1995). In this study, Ca/∑(Si,Al,Fe) ratio and Rb/Sr ratio were used as geochemical proxies for the intensity of authigenic carbonate production, as Rb is considered as a siliciclastic indicator (often associated with clay mineral assemblages), while Sr is a substitute for Ca in carbonate minerals. We assume that high Ca/\(\sum\_{\text{Si,Al,Fe}}\) ratio values and low Rb/Sr ratio values indicate high carbonate authigenic production and thus the lacustrine character of the sedimentary environment, whereas low Ca/∑(Si,Al,Fe) ratio values and high Rb/Sr ratio values indicate low carbonate authigenic production and thus the palustrine or dewatered character of the latter. For periods characterised by a lacustrine sedimentary environment, we assume that decreasing  $Ca/\Sigma(Si,Al,Fe)$  ratio values and increasing Rb/Sr ratio values indicate increasing detrital inputs to the lake basin (An et al., 2018; Campy and Meybeck 1995; Cohen, 2003; Heymann et al. 2013; Koinig et al., 2003; Kylander et al., 2011, Xu et al., 2010) (Appendix B). The Sulphur (S) relative contents were analysed using XRF. We essentially used S relative content as a proxy for anoxic conditions in the lake, which occurred during the highest lake levels (likely to have induced chemical stratification of the water column) and/or during episodes marked by a trophic status of the waterbody inducing predominantly anoxic conditions, such as shallow lake eutrophication. Moreover, in specific sediment bodies and zones, the S relative content may also reflect the presence of gypsum (Bhagowati and Ahamad 2019; Campy and Meybec, 1995; Enters et al., 2010, Gaillard 1995; Hodell et al., 2005a; Qin et al., 2006; Schroder et al., 2018); Wirth et al., 2013) (Appendix B).

The TOC/N ratio was calculated and the  $\delta^{13}$ C value was measured in organic matter (Appendix A). For sediments with high Ca/ $\Sigma$ (Si,Al,Fe) and low Rb/Sr ratios suggesting strong lacustrine carbonate authigenesis, low C/N ratio indicates a significant contribution of OM of algal origin (indicated by the C/N ratio values, Meyers 1994) while low  $\delta^{13}$ C values can be interpreted as land-plant OM with reduced water stress (indicated by the  $\delta^{13}$ C values, Meyers 1994). This signal is therefore an indicator of a relatively lacustrine sedimentary environment (e.g. sediment zone E2B of CS1-S2C, see § 4.3.3.1.1.) (Appendix B).

On the opposite, for sediments with Ca/ $\Sigma$ (Si,Al,Fe) and Rb/Sr ratios suggesting low lacustrine carbonate authigenesis, high C/N values indicate a significant contribution of land-plant-derived OM while high  $\delta^{13}$ C values can be interpreted as an increased water stress (indicated by the  $\delta^{13}$ C values). The C/N ratio and  $\delta^{13}$ C then indicate a more palustrine or dewatered sedimentary environment (e.g. sediment body E3 of CS2-S1, § 4.3.2.2.) (Appendix B). For palaeosoils, higher values of C/N ratio and  $\delta^{13}$ C (with  $^{13}$ C enrichment inducing a  $^{\sim}3$  ‰ increase in  $\delta^{13}$ C) have been interpreted as relating to a relatively dewatered sedimentary environment, favourable to soil pedogenesis, potentially cultivated by plants using the C4 pathway, such as maize (Deines 1980; Farquhar et al. 1982; Krishnamurthy et al. 1982; O'Leary 1981; Webb et al. 2004) (e.g. sediment zone E2A of CS2-S10, § 4.3.1.2.2.) (Appendix B).

Some deposits were studied in thin sections. Microstratigraphic units were defined and described using Bullock et al. 1985 and Stoops and Vepraskas 2003. The description focused on the main and principal pedological, sedimentological, pedo-climatic and ecological features: soil macrostructure and microstructure, groundmass and fabric, presence and type of OM, degree of bioturbation, cryptocrystalline features (Fe and CaCO<sub>3</sub>), illuviation features, presence of ecological features (shells, algae, other).

Complementary to the sedimentary and mineral geochemical approaches, the measurement of the sediment's volumetric magnetic susceptibility (MS) (SI units) was essentially aimed at discriminating between sediment zones of greater or lesser detrital mineralogical fractions, the latter resulting from soil erosion in the watershed (Dearing 1994; Dearing et al. 1987). MS was measured on sediment cores with the MS2 (Bartington) apparatus. Due to the Tertiary carbonate sedimentary beds in the lake basin watershed, the MS values of the lacustrine deposits are low (1 to 18 SI) and the higher values are positively correlated to the higher SiAl+ox contents (materials from detrital inputs).

Within the constituent sediment bodies of the three sediment series, the cross-study of these sedimentological, pedological, geochemical and isotopic markers allowed the identification of sediment zones (SZ). These SZ resulted from fluctuating sedimentary environments and syn- and post-depositional processes (Figs 6, 7, 8).

#### 3.4 Development of the chronological framework of sedimentary deposits

Relative dating was established through the study of the morphostratigraphy of the deposits (Figs 3 and 4) and the study of the artefacts included in the SZ, thanks to the ceramic chronology (Hiquet 2020; Patiño 2013; Perla-Barrera and Sion 2017, 2018). Numerical dating was based on the AMS <sup>14</sup>C dating of 19 samples (Table 1). An AAA (acid-alkali-acid) chemical pre-treatment of these samples removed humic and fulvic acids, and secondary carbonates deposited in organic fractions of sediments (Appendix C). Radiocarbon ages were calibrated using the OxCal v4.4.2 (Bronk Ramsey 2009) according to the atmospheric data from IntCal20 (Reimer P. et al. 2020). In lake systems and carbonated contexts, a hard water effect is possible. This occurs when dissolved carbonates from the watershed enter the lake and are used by aquatic plants (macrophytes and algae) for photosynthesis. In this case, the estimated ages of the OM are older than those that correspond in reality to the time of death of the living organisms from which it was derived ("old carbon" contamination) (Deevey et al. 1954). In this study, when possible, land-plant OM was analysed, such as from charcoal (coal layer) and palaeosoil. In order to assess whether the dates obtained from potentially mixed OM (of

land-plant and aquatic plant origin) were biased by hard-water effect, the ages estimated with land-plant OM (as coal layer) were compared to those estimated with potentially mixed OM. This verification concerned ages included in the same sediment zone or having stratigraphic proximity. Where possible, these ages were also compared with the relative ages indicated by the archaeological material (ceramic sherds) included in the same sediment zone. Age-depth models were calculated for the CS1-S2C, CS2-S1 and CS2-S10 series, using Bayesian chronological modelling with ChronoModel 3.1.2 software (Lanos and Dufresne 2019a, b) (Appendix D). The ages of the sediment zones were calculated using age-depth models (Figs 5 and 11).

#### 3.5 Estimation of mass accumulation rates of mineral fractions

The sediment series of the lakes and bajos of the Petén generally display high vertical variability for the carbonate and silicate fractions (mineral matter, MM) and the organic fraction. The carbonate (CaCO<sub>3</sub>) fraction may be of mixed origin (allochthonous and autochthonous) while the silicate fraction (SiAI) has a detrital allochthonous origin (Beach et al. 2003; Mueller et al. 2009; Rosenmeier et al. 2002a; Wahl et al. 2013, 2014, 2016). The origin, evolution and architecture of these three fractions (CaCO<sub>3</sub>, SiAI, OM) are very different. Therefore, only the accumulation rate values of CaCO<sub>3</sub> (AR<sub>CaCO3</sub>), SiAI+oxides (AR<sub>SiAI+Ox</sub>) and OM (AR<sub>OM</sub>) give an accurate picture of the storage of these phases (Macaire et al. 2006). The variations of AR<sub>CaCO3</sub>, AR<sub>SiAI+Ox</sub> and AR<sub>OM</sub> are mostly independent. They allow a more accurate analysis of the climatic and anthropogenic factors controlling the production of these materials, both on the slopes and in the bajo lake basins. Given the origin of the mineral fractions, the AR<sub>CaCO3</sub>/AR<sub>SiAI+Ox</sub> ratio was estimated in order to evaluate more specifically the proportion of autochthonous carbonate production (see § 3.3 and Appendix B). As the TOC content of these deposits is very low (<1%), the AR<sub>OM</sub> was not considered. The methodology adopted to estimate the AR is presented in Appendix E.

#### 3.6 Palaeohydrographic and palaeohydraulic estimates

The reconstructed water bodies (surfaces and volumes) were modelled using interpretations of stratigraphic, sedimentary, chronological and altimetric (LiDAR) data. The geometry of the sediment bodies of the lake depression (basin stratigraphic architecture, altitude of the top of the nearshore zones deposits), the lithofacies (alluvium, calcareous tuffs) and the chronological markers, made it possible to propose 1: palaeobathymetric lines, 2: the location of the ancient shoreline zones and 3: the minimum altitude of the seasonal high-water level (SHW) (Figs 3 and 4). The volume of lake water corresponding to each reconstructed water level was calculated (Appendix F).

# 4. Results

#### 4.1 Current hydrological dynamics of the lake depression of the polje

Five swallow holes (called *resumideros*) or ponors were identified within the lake depression, at the footslope of the *bajo* hills (S1 to S5, Fig. 1). They contribute to water outputs and probably also to inputs.

#### 4.1.1 Hydrological measurements of the seasonal alternation of high-water level and dewatering

From May 2015 to April 2019, the *civales* were dewatered most of the time. The interannual variability of flood duration was significant, ranging from 25 to 107 days/year, i.e., from 7 to 29% of the time (Fig. 2A). In some years, such as 2016/2017, a second episode of flooding was observed in late June and early July. The maximum depth of the water body was 0.65 m, for a surface area of 21.5 ha and a water volume of 57,200 m<sup>3</sup>. The maximum water level was reached very quickly after the start of flooding (5 to 30 hours). Dewatering was marked by a gradual decrease in water levels, lasting several weeks or months depending on the hydrological year. During the studied period, flood duration, as well as the associated average depths of the intermittent lake, decreased gradually during the first three years, reaching a minimum at the end of 2017, beyond which they increased. Furthermore, the seasonal thermal amplitude of the water located 6 m below the ground surface

(piezometer water, probe P1) was low (~0.5 °C). Temperatures varied according to positive and negative seasonal deviations from a multi-year temperature trend (Fig. 2A).

#### 4.1.2 The lichen trimline and high watermarks: evidence of hydrological years with seasonal very

#### high-water levels

352

353

354

355

356

357

358

359

360

361

362

363

364

365

366

367

368

369

370

371

372

373

374

375

376

During the hydrological years 2012-2013 and 2013-2014, field observations showed that the lake high-water levels were higher than those of the period 2015-2019. At the end of the dry season, the maximum depth of the lake exceeded 0.4 m in 2013 and 1 m in 2014. The study of lichen trimlines and high-water marks allowed for the characterisation of previous hydrological dynamics.

A Corticolous Crustose Lichen Trimline (CCLT) was observed at seven of the 16 studied stations (Fig. 2B). The stations with CCLT are all located within the lake depression while the others are all located in the bajo, outside this depression. The mean value of the CCLT altitude is estimated at 267.64 +/-0.1 m a.s.l. The similarity of the CCLT altitude on trees several hectometres apart and at different altitudes is interpreted as the effect of prolonged immersion on lichen survival. Lichen trimlines occur where a high-water level lasts for a prolonged period, during which time the submerged lichens die and fall off the substrate (Hale 1984; Rosentreter 1992). According to an experimental study (Marsh and Timoney 2005), the average mortality of lichens increases after about one month of immersion, reaching 68% in three months, 91% in six months and 100% in nine months. The CCLT characterised in this study could mark the altitude of the water levels reached during one or more long-duration seasonal floods, lasting for more than six or nine, or even 12 months. Moreover, the altitude of the high watermarks observed in the western civale is estimated at 267.56 +/- 0.15 m a.s.l. The convergence of the results obtained by these two independent methods reveals that this lake depression experienced one or more episodes of seasonal very high-water levels (SVHW), in recent years (prior to 2013) or decades. The most recent one(s) occurred less than 15 years ago, as evidenced by the age of the youngest trees at the stations with CCTL. The maximum depth of the

intermittent lake formed during SVHW was 2.55 +/- 0.15 m, its surface area 70 +/- 4 ha and its

volume 892,000 +/- 105,000 m<sup>3</sup> (Figs 10 and 11). During the SVHW years, the lake was probably not seasonally dewatered and the altitude of the lake basin mouth was not reached.

**Fig. 2.** Current seasonal and interannual fluctuations of the El Infierno intermittent lake hydrosystem, revealed by the study of piezometric data (2A), the lichen trimline and the high watermark (2B).

#### 4.2 Stratigraphy and chronology of the sedimentary filling of the lake basin

#### 4.2.1 Morpho-stratigraphy of alluvial and colluvial fill

#### 4.2.1.1 Western stratigraphic cross-section (CS2)

The filling of the lake basin consists of four main sediment bodies (E1 to E4) (Fig. 3), each of which comprises subsections named sediment zones (E1A, E1B, etc.) (Figs 6 and 7). The thickness of the deposits is greatest in the centre of the basin, where it exceeds 4.5 metres. E4 is the oldest and the most extensive. E3 is nested in E4. E2 and E1 are superimposed on E4 and E3. E1 and E3 consist of weakly carbonated alluvial and colluvial silty clay, whereas E2 and E4 contain carbonated alluvial and colluvial clayey silt. E1, E2 and E3 include palaeosoils. They have a relatively tabular structure and are bevelled at the margins of the basin. At the opposite ends of each sediment body, the altitudes of the top of the bevels are the same (+/- 0.1 to 0.2 m). This observation is also valid when comparing the altitude of the bevels of the same sediment body between CS2 and CS1 (Figs 3 and 4). This results from hydro-sedimentary processes in palustrine and lake environments (Talbot and Allen 1996; Miall 2000). The deposits of E1 and to a lesser extent those of E2 and E3, show multi-decimetric post-depositional deformations. These are related to argilliturbation. The seasonal alternation of wetting and drying of soils and superficial deposits, and their consequences on expansion-contraction processes, have been described regionally (Beach et al. 2003; Dunning et al. 2002).

Fig. 3. West stratigraphic sections (CS2 and CS2-S10) of the El Infierno lake basin and its margins.

#### 4.2.1.2 Eastern stratigraphic cross-section (CS1)

The stratigraphic architecture and lithofacies characterised in CS1 are relatively similar to those in CS2 (Fig. 4). Nevertheless, here the basin is asymmetric. The maximum fill (~ 6 metres) is near the foot of the hillslope, where the *civale* is located. The geometric relationships between the alluvial sedimentary subset (E2) and the colluvial subset (E2"), reflect a lateral variation in the lithofacies of E2. The colluvium (E2") is essentially calcareous and relatively coarse (sandy gravel with or without a silty matrix and pebbles). The deposits of E1 were also affected by post-depositional deformation.

**Fig. 4.** East stratigraphic sections (CS1, Southern margin section, CS1-TER and CS1-S2C) of the El Infierno lake basin and its margins.

#### 4.2.2 Age of deposits and chrono-stratigraphic interpretations

Comparison of the ages estimated by the radiocarbon method on land-plant OM with those estimated on potentially mixed OM (of land-plant and aquatic plant origin) and/or with the ages of the archaeological material (ceramic sherds) revealed a chronological coherence within and between the sediment zones of each series. No hard water effect was identified in the whole dataset studied (Table 1). The amount of radiocarbon dates on charcoal and OM from paleosoils, as ell as the intermittent dynamics of the lake system may explain this coherence.

The morpho-stratigraphy and chronological markers allowed the following chrono-stratigraphic interpretations. E4, the top of which is dated to around [3522-3193] BCE in CS2-S1, has a mid-Holocene and possibly also early Holocene age (Figs 3, 4, 11). E3 starts in the mid-Holocene, between [3522-3193] and [3262-2906] BCE. The E3/E2 transition occurred in the Late Holocene, shortly after [1536-1301] BCE and before [1372-933] BCE according to CS2, and shortly before [1441-1272] BCE according to CS1. The E2/E1 transition is significantly earlier at the edges of the lake depression (dated between ~350 and 50 BCE according to CS1 and CS2) than in the centre [dated around ~1250 CE (after 893-1026 CE)]. Isochronous lines (palaeobathymetric profiles) are reconstructed for five moments: ~3500 BCE, 1500-1400 BCE, 400-200 BCE, 200-400 CE and 900-1020 CE (Figs 3 and 4).

- 427 Table 1. Radiocarbon ages. Calibration: see text (§ 3.4). Poz: Poznań Radiocarbon Laboratory. Beta: Beta Analytic testing
- 428 laboratory. Depth b.s.: below surface. Numbers in brackets: rejected age.
- 429
- 430 Fig. 5. Age-depth models of the sediment series CS2-S1, CS2-S10 and CS1-S2C.
- 431
- 4.3 Sedimentology, pedology, geochemistry and accumulation rates of deposits. 432
- 433 4.3.1 Sediment serie CS2-S10 (western section – basin margin)
- 434 Three sediment bodies (E1 to E3) are distinguished (Figs 3 and 6).
- 4.3.1.1 Sediment body 3 (E3): 210 to 160 cm 435
- 436 The silty clays of E3 are the finest in this sediment series and are similar to the E3 deposits described
- 437 in CS2-S1. These lutites were deposited in stagnant-water environments. CaCO₃ contents, the Ca/∑
- 438 (Si,Al,Fe) ratio and relative contents of Ca and sulphur (S) are the lowest of CS2-S10. The Rb/Sr ratio,
- 439 relative content of terrigenous detrital elements (Ti, Fe, Zn, Zr, Rb, Pb), which are markers of
- 440 mechanical erosion, and magnetic susceptibility (MS) values are the highest. The contribution of
- 441 carbonate authigenesis was therefore relatively low and terrigenous detrital inputs were high.
- 442 Nevertheless, the C/N ratio suggests a terrestrial and aquatic contribution to the OM. The E3 facies is
- 443 typical of a vertisol with shrink-swell processes (slickensides and wedge-shape peds) (palaeosoil Sb,
- 444 Fig. 3). At the top of E3, the porosity and presence of OM suggest in situ vegetation development.
- 445 The proportion of diverse oxidation features (Mn coatings, Fe and Mn impregnation, Mn
- hypocoatings) suggests, together with the granular microstructure, repeated wetting and drying 446
- 447 cycles with several days of water saturation (Hussein and Adey, 1998). The sediment environment
- 448 was relatively dewatered, pedogenized, slightly alkaline and slightly reducing compared to those of
- E2 and E1. 449
- 4.3.1.2 Sediment body 2 (E2): 160 to 112 cm. 450
- The clayey silts of E2 are the coarsest of CS2-S10. CaCO<sub>3</sub> (%), Ca (count s<sup>-1</sup>) and Ca/ $\Sigma$ (Si,Al,Fe) values 451
- 452 are the highest of this series, unlike Rb/Sr and MS. Relative S contents are higher and oxidation

features are less numerous than in E1 and E3. E2 is a tufaceous limestone. A palaeosoil developed at the top of E2. In CS2-S10, as in CS2-S1 and CS1-S2C, the grain-size distribution of the deposits depends more on the fraction of carbonate authigenic minerals than on the energy of the sediment environment. There is a positive correlation between the silt fraction (%) on the one hand and the CaCO<sub>3</sub> (%) and Ca (count s<sup>-1</sup>) on the other hand. Moreover, during periods of increased erosion and sediment transfer (see § 5.2), alluvial deposits were no coarser.

#### 459 4.3.1.2.1 Zone E2B (160 – 124 cm)

453

454

455

456

457

458

460

461

462

463

464

465

466

467

468

469

470

471

472

473

474

475

E2B is typical of lacustrine limestones, mainly due to the presence of faunistic and floristic content, such as traces of whole shells, fish bones, and alga oogones (Freytet and Verrecchia 2002). The biogenic precipitation of carbonate is responsible for the identified micritic and microsparitic lacustrine muds, as confirmed by the presence of mollusc shells and calcified algae. The identification of laminae in the micritic deposits suggests formation below the wave in a calm environment (Digerfeldt et al. 2007; Huber and Ismail-Meyer 2012). E2B is multi-phasal (E2B1 to E2B4). Granular to vughy structures (E2B1, E2B3) alternate with platy to subangular blocky structures (E2B2, E2B4). C/N values are low and include the minima of CS2-S10. E2B1 and E2B3 are more carbonate- and Srich and deprived of traces of oxidation. In addition, most of the vughy structured deposits are observed in E2B1 and E2B3, and have a cristallitic b-fabric (laminated micritic to microsparitic muds), numerous fragments of whole and broken shells, as well as Characeae oogones (a macroalga found in many carbonate-rich aquatic systems). The sediment environment corresponds to that of a perennial alkaline water body (Fig. 6). E2B2 and E2B4 and the top of E2B1 have lower S contents and higher oxidation-reduction traces. The carbonate tufa of E2B4 includes centimetric and millimetric beds of silty clay. The sediment environment was temporarily dewatered and also experienced increased detrital inputs.

#### 4.3.1.2.2 Zone E2A (124 – 112 cm)

The clayey silts of E2A show traces of pedogenesis and include artefacts (ceramic sherds) (palaeosoil Sa, Fig. 3). The deposits and their micro-structure (b-fabric) are lacustrine marl. But the presence of rounded carbonate pelloids and marmorization are typical of vertisol conditions with shrink-swell cycles. While the matrix presents a greyish colour typical of a water-saturated environment, the mottled features resulting from the accumulation of OM and the formation of redox features suggest a well-aerated soil. Increased oxidising conditions are also indicated by the decrease in relative S content and the numerous diffuse traces of iron impregnations and orthic manganese nodules. Soil structure and content in OM are indicative of the development of in situ vegetation associated with the exposure of the sediments (dewatered environment). The C/N ratio and  $\delta^{13}$ C reach the highest values of CS2-S10 (Fig. 6), indicating an increased contribution of terrestrial origin OM. The  $\delta^{13}$ C values (-19 ‰ and enrichment of 3 ‰ compared to E2B and E1) reveal that part of the OM in this palaeosoil originated from C4 plants and probably indicates maize cultivation, an inference supported by the identification of maize-associated phytoliths in this level by Testé (2020).

#### 4.3.1.3 Sediment body 1 (E1): 112 to 0 cm.

The silty clays of E1 present features typical of vertisols associated with a carbonated matrix. E1B (transition unit from E2A to E1A) is characterised by decreasing relative Ca contents and  $Ca/\Sigma(Si,Al,Fe)$  ratio and increasing Rb/Sr ratio. Relative S contents decrease and numerous traces of oxidation features are recorded. The environment is more dewatered and oxidizing than in E2. The intra-aggregate granular structure indicates repeated wet and dry cycles (Hussein and Adey 1998), but the preservation of illuviation features also indicates a reduced number of shrinking and swelling cycles. This is in accordance with the various and diverse oxidation features pointing towards repeated wetting and drying cycles and phases of complete evaporation (Lindbo et al. 2010). The silty clays of E1A include  $CaCO_3$  contents and  $Ca/\Sigma(Si,Al,Fe)$  ratio, lower than E2 and higher than E3. Conversely, the Rb/Sr ratio and MS are higher than in E2 and lower than in E3.

501 Fig. 6. Stratigraphy, sedimentology, geochemistry and micromorphology as well as <sup>14</sup>C age estimates of the CS2-S10 series. 502 503 4.3.2 Sediment serie CS2-S1 (western section – centre of the basin) 504 Four sediment bodies are distinguished (E4 to E1) (Figs 3 and 7). 505 4.3.2.1 Sediment body 4 (E4): below 440 cm 506 Only the top of E4 was analysed. All CS2-S1 deposits are lutites. E4 has high values of relative Ca, 507 Ca/∑ (Si,Al,Fe) ratio and S contents and low values of Rb/Sr and C/N ratios. The values of 508 Ca/\(\sum{\subset}(Si,Al,Fe)\) ratio are the highest of CS2-S1. Carbonate authigenesis in an alkaline reducing aquatic 509 environment largely contributed to this deposit. 510 4.3.2.2 Sediment body 3 (E3): 440 to 308 cm The silty clays of E3 are the finest deposits of CS2-S1, CS2-S10 and CS1-SC2. They have a vertisol 511 512 (slickenside) soil structure (palaeosoil Sb', Fig. 3). The CaCO<sub>3</sub> content and Ca/ $\Sigma$ (Si,Al,Fe) ratios are the 513 lowest of CS2-S1, while the Rb/Sr ratio and SM values are the highest. This reflects a strong 514 contribution of terrigenous detrital inputs and a low authigenic contribution. The C/N values are the 515 highest of those observed in CS2-S1, indicating a relatively high contribution of terrestrial OM. E3 516 does not include calcareous bioclast such as mollusk shells. The E3 environment was less alkaline and 517 more dewatered than in E4 and E2. 518 4.3.2.3 Sediment body 2 (E2): 308 to 70 cm The lutites of E2 are the coarsest of CS2-S1. CaCO₃ and Ca contents and Ca/∑(Si,Al,Fe) ratio are the 519 520 highest, while Rb/Sr ratio and MS are the lowest. Authigenic carbonate production is significantly 521 higher. The silty texture of the authigenic minerals contributes to the increased D50. Nevertheless, 522 terrigenous inputs contribute to the majority of the deposition. In E2, the measured C/N (7-13) and 523  $\delta^{13}$ C (between -25 and -22.5 %) are lower than in E3. Relative S contents are generally higher in E2 524 than in E1 and E3, presumably related to relatively more reducing conditions. E2 includes calcareous bioclasts such as mollusk shells. The environment was among the most aquatic and alkaline of the
 series. Four main zones (E2A to E2D) are distinguished.

4.3.2.3.1 Zone E2D (308 – 220 cm)

527

- E2D is marked by a strong concomitant increase in  $CaCO_3$  content,  $Ca/\sum(Si,Al,Fe)$  ratio and S content, 528 529 while Rb/Sr and MS values decrease. At the E3/E2 transition, the C/N ratio decreases markedly (from 13-15 to 7-11) while  $\delta^{13} \text{C}$  is relatively constant. The deposit evolves into a clayey silt. E2D includes 530 531 laminated (millimetric) deposits. This reflects an increased contribution of authigenesis to deposition, 532 in a more alkaline and reduced aquatic environment, and a relative decrease in the allochthonous terrigenous detrital contribution. Some of the deposits of E2D may have been emplaced in a 533 534 perennial aquatic environment. Furthermore, the Ca/∑(Si,Al,Fe) and Rb/Sr ratios fluctuate with a 535 rather strong amplitude (alternation of five to six successive peaks) and are negatively correlated. 536 This possibly suggests the succession of periods marked by alternating high and low frequencies, 537 durations and heights of lake floods and/or by variations in detrital inputs.
- 538 4.3.2.3.2 Zone E2C (220 177 cm)
- E2C is marked by an increased Rb/Sr ratio and decreased CaCO<sub>3</sub> content, Ca/∑(Si,Al,Fe) ratio and S content. However, the values do not reach those of E3 or E1. The clay fraction is clearly increased. In contrast to E2B and E2D, E2C contains traces of pedological evolution (palaeosoil Sa', Fig. 3). The environment was relatively less aquatic and alkaline and possibly marked by increased detrital input.
- 543 4.3.2.3.3 Zone E2B (177 100 cm)

544

545

546

547

E2B shows a high CaCO<sub>3</sub> content and Ca/ $\Sigma$ (Si,Al,Fe) ratio. Rb/Sr ratio and MS values vary in opposite ways and reach lower values than E2D. The C/N ratio (9-13) and  $\delta^{13}$ C values are relatively low. ED2 evolves into a clayey silt and includes laminated deposits (like E2D). The interpretation is comparable to that of E2D.

4.3.2.3.4 Zone E2A (100 – 70 cm)

E2A is marked by a decrease in  $CaCO_3$  content,  $Ca/\Sigma(Si,Al,Fe)$  ratio and an increase in Rb/Sr ratio. The deposit evolves towards a silty clay. E2A thus experiences a polyphase drop in the contribution of carbonate authigenesis to sedimentary deposition in a less alkaline aquatic environment than in E2B. This trend is particularly marked in E2A2. Subsequently, E2A1 shows a peak in  $CaCO_3$  content and values of  $Ca/\Sigma(Si,Al,Fe)$  ratio and low values of Rb/Sr ratio. The sedimentary environment of E2A1 was possibly marked by significantly increased frequencies, durations and heights of floods compared to those of E2A2.

#### 4.3.2.4 Sediment body 1 (E1): 70 to 0 cm

- The  $CaCO_3$  content and  $Ca/\Sigma(Si,AI,Fe)$  ratio are low and the Rb/Sr ratio increases. This probably reflects the drop in the contribution of carbonate authigenesis to sedimentary deposition in a less alkaline environment.
- **Fig. 7.** Stratigraphy, sedimentology and geochemistry as well as <sup>14</sup>C age estimates of the CS2-S1 series.

4.3.3 Sediment serie CS1-S2C (eastern section – basin margin)

- Two sediment bodies (E1 and E2) and five zones are distinguished. All zones include artefacts, excluding E1A (Figs 4 and 8).
- 565 4.3.3.1 Sediment body (E2): 256 to 166 cm
  - Between 256 and 246 cm, E2 presents a layer of coarse calcareous colluvium (E2C). Later, E2 is characterised by clayey silts, which are the coarsest and most carbonated of CS1-M2C (E2A and E2B). The allochthonous minerals are mainly clays while the autochthonous minerals are mainly calcite crystals (micrite, sparite) with the texture of very fine and fine silts. The Ca/\(\Si\)(Si,Al,Fe) ratio is the highest while the Rb/Sr ratio is the lowest. E2A and E2B are marked by the highest contribution of authigenesis and the lowest detrital inputs in the series, as well as in its lower part, by the most aquatic alkaline sedimentary environment.

#### 4.3.3.1.1 Zone E2B (246 – ~196 cm)

E2B is distinguished from the other zones by bedded deposits, marked by alternating light and dark centimetric beds (see P2, P3 of CS1-S2C section, Fig. 4). Low C/N ratio values are associated with the lowest  $\delta^{13}$ C values measured in CS1-S2C. The presence of S could reflect more reducing conditions than in E2A and E1B. The light beds have a higher relative content of Ca and S. These beds are probably the result of hydrological fluctuations [frequencies, durations and heights of lake floods, alternating high (light beds) and low (dark beds)]. This alternation of beds is nevertheless possibly the result of variations in detrital inputs. The top part of E2B (and laterally in the stratigraphic section) includes the bevel of the Co2 colluvial layer, which contains artefacts (Fig. 4).

## 4.3.3.1.2 Zone E2A (~ 196 – 166 cm)

E2A is marked by a strong polyphase increase in detrital markers and a decrease in authigenesis [increase in Rb/Sr ratio and MS (two main peaks of CS1-S2C) and a joint decrease in the Ca/ $\Sigma$ (Si,Al,Fe) ratio (Fig. 8)]. Laterally in the section, E2A includes the bevel of the Co1 colluvial layer which contains artefacts (Fig. 4). E2A also shows increased and fluctuating C/N ratio values, suggesting an increase in the fraction of terrestrial origin OM. In this context, the small increase in  $\delta^{13}$ C (+0.5 to +1 %) is interpreted as a shift towards relatively less aquatic conditions (isotopic enrichment due to increased water stress).

#### 4.3.3.2 Sediment body (E1): 166 to 0 cm

E1 is composed of E1A and E1B zones.

#### 592 4.3.3.2.1 Zone E1B (166 – 51 cm)

E1B is more clayey than E2 with large shear planes (slickensides) associated with vertisol-type pedogenesis and multi-decimetric to metric deformation of the deposits (argilliturbation). The CaCO<sub>3</sub> content and Ca/ $\Sigma$ (Si,Al,Fe) ratio are significantly lower than in E2, inversely to the Rb/Sr ratio. The S content is zero, suggesting oxidising conditions.  $\delta^{13}$ C still displays some of the highest values of E1B and E2, while the C/N ratio is lower than that of E2B, reflecting a significantly increased contribution

of algal OM. The contribution of detrital inputs to sediment deposition is high. The environment was relatively more aquatic than in E2A but regularly subject to dewatering.

#### 4.3.3.2.2 Zone E1A (51 – 0 cm)

The silty clays of E1A are the finest of CS1-S2C. A histosol is currently developing at the top of E1A. The  $CaCO_3$  content and  $Ca/\Sigma(Si,Al,Fe)$  ratio are the lowest of this series, while the Rb/Sr ratio is by far the highest. The deposition of these deposits probably took place in a very weakly alkaline environment. Inputs are mainly detrital. Authigenesis is very limited. Nevertheless, the presence of S in E1A could suggest an evolution towards relatively more aquatic conditions than in E1B.

Fig. 8. Stratigraphy, sedimentology and geochemistry as well as <sup>14</sup>C age estimates of the CS1-S2C series.

#### 4.3.4 Accumulation rates of mineral fractions

The accumulation rates of mineral matter ( $AR_{MM}$ ) of CS2-S1 and CS2-S2C are higher than those of CS2-S10 because these first two series are located at the bottom of the lake depression. The  $AR_{MM}$  of the fine deposits of these first two series evolved in six distinct periods ( $AR_1$  to  $AR_6$ ); three periods marked by high  $AR_{MM}$  ( $AR_1$ ,  $AR_3$ ,  $AR_5$ ) alternating with three periods marked by relatively low  $AR_{MM}$  ( $AR_2$ ,  $AR_4$ ,  $AR_6$ ) (Fig. 9). During the past five millennia, the lowest  $AR_{MM}$  were observed between ~2300 and ~1600 BCE whereas the highest were observed between ~3500 and 3000/2900 BCE, ~850 and ~100 BCE, and again between ~500 and ~ 1000 CE. The fluctuation of ARs is such that the ratio of maximum to minimum values for  $AR_{MM}$  and  $AR_{SIAI+OX}$  is around 4, while that of  $AR_{CaCO3}$  reaches 9. The  $AR_{SIAI+OX}/AR_{CaCO3}$  ratio fluctuated between 1.5 and 15. Between ~1500 BCE and ~1200 CE, the  $AR_{CaCO3}/AR_{SIAI+OX}$  ratio was high. Its values were often 2 to 3 times higher than those observed before and after this period (Fig. 9). The interpretation of AR variability will be discussed in relation to hydro-sedimentary fluctuations (see below § 5.2 and 5.3).

**Fig. 9.** Evolution of mass accumulation rates (AR) of mineral fractions of the fine deposits and evolution of the AR<sub>CaCO3</sub>/AR<sub>SiAl+Ox</sub> ratio, in the El Infierno lake basin during the past 5500 years. MM: mineral matter. SiAl+Ox: silicate fraction and oxides. CaCO<sub>3</sub>: carbonate fraction. Green bands (light/dark) = relatively low AR<sub>MM</sub> (low/very low); Yellow bands (light/dark) = relatively high AR<sub>MM</sub> (high/very high).

# 5. Discussion

5.1 Current baseline of seasonal and interannual hydrological variability: nature and

# 628 forcing

626

627

629

630

631

632

633

634

635

636

637

638

639

640

641

642

643

644

645

646

647

648

649

650

651

As far as we know, this study is the first to provide, in the SMLs, quantitative information on the current hydrological regimes of the *civale* hydrosystems, on the current inundation areas of karst poljes and, at the same time, to examine their forcings by climate, geomorphology and vegetation.

#### *5.1.1 Control of the seasonal variability of intermittent hydrological dynamics.*

Currently, this lake is ephemeral, i.e. holds water intermittently, according to the definition proposed by Ravbar et al. (2021), and based on the extent, duration and frequency of flooding. From 2015-2019, the main floods occurred each year in response to the second peak of precipitation (P) of the rainy season (September-November), when air temperatures (T) dropped significantly below the annual average, in October and November (Fig. 2A). At this time, the P/ETP ratio (precipitation/evotranspiration), as well as moisture storage and possible ground water storage (local perched groundwater), were higher than those at the first part of the rainy season. This explains why the hydrological response rarely resulted in lake flooding during the first rainy season peak, or only a brief and low-level flood (Fig. 2). After the peak of the flood, the decrease in lake level until total dewatering resulted in several consecutive weeks to months of negative hydrologic budget, due to the decrease in P and the increase in ETP (with increase in T under similar vegetative conditions). The dewatering of soils and superficial deposits of the bajo was maximal at the end of the dry seasons (Fig. 2A). Therefore, these present civales are perennial wetlands, similar to others in Petén (Dunning et al. 2002; Lundell 1937). Their lacustrine hydrological regime reflects intermittent dynamics controlled by the regional climate. Moreover, the seasonal negative deviations from the multi-year trend of the piezometer water temperatures were positively correlated with the positive seasonal deviations from the multi-year average of air temperatures (Fig. 2A). This indicates a response to the increased seasonal intensity of ETP, its endothermic thermodynamics properties and their thermal consequences for the bajo soils and superficial deposits, subject to seasonal wetting-drying alternation. These processes contribute significantly to argolliturbation, as described here and more widely in the Petén and tropical zone (Beach et al. 2003).

#### 5.1.2 Control of interannual variability of hydrological regimes

652

653

654

655

656

657

658

659

660

661

662

663

664

665

666

667

668

669

670

671

672

673

674

675

The interannual variability of the lake's hydrological dynamics is strong and is characterised by two alternating hydrological regimes. The first is a seasonal high-water level regime (SHW), characterised by a duration of flooding of less than three months, a maximum lake depth inferior to 0.5 m and an annual flood frequency of 1. The second is a regime of seasonal very high-water level (SVHW), characterised by a duration of flooding longer than three months (which can exceed six months and sometimes one year), a maximum lake depth greater than 0.5 m (which can reach 2.5 m) and an annual flood frequency higher than or equal to 1 (Figs 2 and 10). During the 2015-2019 period, which was characterised by SHW regimes, the seasonal decrease in the duration and depth of the lake's floods was positively correlated with the seasonal increase in water temperatures (Fig. 2A). This suggests a control of the interannual variability of the hydrological dynamics by the interannual variability of the thermal and rainfall regimes. The hydrological variations of this lake possibly evolve in a cyclical manner, with a half-period longer than three years. This may reflect the response to interannual variability in rainfall patterns of the regional climate (Enfield and Alfaro 1999; Giannini et al. 2000; Taylor et al. 2011, 2002). The earlier period was dominated by SVHW regimes [during 2012/13 and 2013/14 and for some years before this (more recent than ~2000 CE)]. SVHW regimes may have been controlled by hydrological years with cooler and wetter climate conditions and/or hurricane occurrence. Seasonal lake levels are also constrained by geomorphological control, by swallow holes or ponors. During the years marked by a SHW regime, seasonal high-water levels (265.4 to 265.8 m a.s.l.) were at the same altitude as the top of four swallow holes or ponors (265.6 +/- 0.2 m for S1 to S4, Figs 1

and 10). During years with SVHW regime, water levels were constrained by the five swallow holes or

ponors (S5 altitude of 266.9 +/- 0.1 m a.s.l.). This control is commonly encountered in karst contexts (Ford and Williams 2007; Ravbar et al. 2021; Salomon 2006).

The analysis of the current lacustrine hydrological regime and its driving factors (climatic, geomorphological, biogeographical and anthropogenic) reveals that the latter is mixed, of karstic and evaporative type. This hydrosystem is currently endorheic but it has influent seepage. Concerning lacustrine inputs, the dissolved load of water is due to chemical erosion of the geological formations. But the current average residence time of the water in this lake is short (often less than three or six months). These characteristics limit the influence of lake processes, such as the precipitation and the accumulation of carbonates and the sedimentation of fine particles (Meybeck 1995). The current baseline of this hydrosystem thus reveals that it is particularly sensitive to biophysical and climatic parameters that may impact its hydrologic budget.

**Fig. 10.** Map of hydrological and palaeohydrological dynamics of the El Infierno lake basin, of resource use and management and of settlement by the ancient Maya in its watershed during Preclassic and Classic periods.

- 5.2 Multi-centennial and multi-millennial variability in Holocene hydro-sedimentary
- 691 dynamics: nature and forcing.
- Seven main hydrological periods (HP1 to HP7) and five major erosion and sediment transfer periods
- 693 (ESTP1 to ESTP6) occurred over the past six millennia (Fig. 11).

**Fig. 11.** Synthesis of the hydrological and sedimentary dynamics of the El Infierno bajo lake basin during the past 5500 years, in responses to anthropogenic and climate drivers. Blue vertical bands: periods of relatively high lake levels. Blue dashed horizontal lines: frequently perennial lake; red dashed horizontal lines: frequently dry lake. Brown vertical bands: periods of increased erosion and sediment transfer. Higher Ti content is interpreted by Haug et al. (2001) to indicate greater precipitation.

#### 5.2.1 Pre-anthropogenic baseline of hydro-sedimentary dynamics under climate control, between

~3500 and ~1500 BCE

#### 5.2.1.1 Hydrological period 1: before ~3500 BCE

HP1 was marked by the highest lake levels, indicated by the architecture and lithofacies of the deposits (E4 of CS2-S1, Figs 3 and 7). The altitude of the top of E4 corresponds to that of the lake basin mouth (Figs 3, 4, 10). The lacustrine depression was filled at least seasonally and possibly supported a perennial lake. Water outputs through the basin mouth are not demonstrated for later hydrological periods. Lake water volumes were ~4.07 +/- 0.23 .10<sup>6</sup> m³ (Fig. 11). The regional climate of the early to mid-Holocene period was warmer and wetter than that of the Late Holocene (Hodell et al. 1991, 1995; Islebe et al. 1996). It controlled this high lake level of the Petén lakes, such as Puerto Arturo Lagoon (Wahl et al. 2014), Lake Paixban (Wahl et al. 2016), and Lake Petén Itzá (Mueller et al. 2009) for the period from ~7000/6000 to ~3000/2500 BCE.

#### 5.2.1.2 Hydrological period 2: from ~3500 to ~1500 BCE

HP2 was marked by low lake levels indicated by lithofacies (E3 of CS2-S1 and E3 of CS2-S10, Figs 6, 7, 10) and the architecture of E3 nested within E4 (Figs 3 and 4), low AR<sub>MM</sub> and AR<sub>CaCO3</sub>/AR<sub>SIAl+Ox</sub> ratio (AR<sub>2</sub>, Fig. 9), and a phase of pedogenesis (palaeosoils Sb, Sb', Fig. 3). Multi-decadal or multicentennial phases of dewatering may have occurred during this period. During the HP1/HP2 transition, evidence of anthropization in the EIR is sparse and suggests low impacts on EIR environments and is absent at Naachtun (Castanet et al. 2021). Many references indicate an initial or accelerated decline of the forest, later, between ~2000 BCE and 1000 CE (Jones, 1991; Islebe et al, 1996; Leyden et al. 1998; Wahl et al. 2006). The HP1/HP2 transition and HP2 were forced by the climate. A drop in lake levels has been described regionally, around 2500 BCE in Lake Petén Itzá (Mueller et al. 2009), 3500 BCE in Lake Paixban (Wahl et al. 2016) and between 4300 and 2500 BCE in Puerto Arturo (Wahl et al. 2014). The latter may have remained low between 2700 and 1400 BCE,

and that of Paixba between 3500 and 1750 BCE. These drops have been related to a transition to a drier regime climate since ~3450 BCE (Haug et al. 2001) (Fig. 11).

727

736

741

742

743

744

745

746

747

748

749

- 728 5.2.1.3 Erosion and sediment transfer periods 1 and 2: from  $\sim 3500$  to  $\sim 1500$  BCE.
- ESTP1 and ESTP2 were characterised by the lack of coarse colluvium at the foot of the *bajo* hillslope
  (Fig. 11). During ESTP2, the very low alluvial AR<sub>MM</sub> values suggest biostatic conditions marked by
  morphogenic stability. This very low-intensity soil erosion and sediment transfer did not occur again
  after this period. They were related to low or no anthropogenic impacts on forest cover and soil. The
  lowest lake sedimentation rates of the Holocene occurred during this period in lakes Petén Itzá
  (Mueller et al. 2009) and Salpetén (Rosenmeier et al. 2002a, 2002b). ESTP1 was characterised by
  greater alluvial AR<sub>MM</sub> and may have resulted from wetter Atlantic period climatic conditions (Haug et
- 737 5.2.2 Hydro-sedimentary dynamics under climatic and Maya anthropogenic control, from ~1500
- 738 BCE to ~1000/1150 CE
- 739 5.2.2.1 Period ~1500 BCE ~300/100 BCE.

al. 2001; Hodell et al. 1991).

- 740 5.2.2.1.1 Hydrological period 3 (~ 1500 ~ 300 BCE)
  - HP3 began with a lacustrine transgression revealed by prograding sequences on the margins of the depression and continued with high lake levels. E2 overlays E3 and part of E4 (Figs 3 and 4). Alkaline shallow lake lithofacies are observed in E2D of CS2-S1, E2B of CS2-S10 and E2F to E2B of CS1-S2C (Figs 6, 7, 8). Increased AR<sub>MM</sub> result from increased lacustrine carbonate authigenesis and alluvial detrital inputs (upper AR<sub>2</sub> and AR<sub>3</sub>) (Fig. 9). The lake was probably sub-perennial to perennial, from ~1225 to ~1050 BCE (E2B3 of CS2-S10) and then from ~710 to ~440 BCE (E2B1 of CS2-S10). The latter episode (~710-440 BCE) shows the strongest evidence of a perennial lake. The variability of the lithofacies described in E2B of CS1-S2C (Figs 4 and 8) and E2D of CS2-S1 (Figs 3 and 7) suggest fluctuating lake levels and/or detrital inputs with periods averaging between 50 and 100 years. Lake

water volumes estimated for HP3 were about a third of those in HP1, but were "three times greater than present-day volumes (Fig. 11). No wetter regional climate events are identified during the HP2/HP3 transition (Douglas et al. 2016). In contrast, Petén lake geochemical and biological indicators point to a drier episode around 1500 BCE (Mueller et al. 2009) and around 1000 BCE (Wahl et al. 2014) and, more broadly, severe drought between 1500 and 500 BCE (Douglas et al. 2016). The first evidence of settlement and land use in the study area are multiple: colluvial deposits between ~ 1500 and 800 BCE (Co5 to Co3, Fig. 4), artefacts (ceramic sherds) in colluvium and alluvial palaeosoils (Figs 3 and 4), archaeological evidence of Middle Preclassic occupation at Kunal located 4.5 km from the lake (Nondédéo et al. in press, 2020a) and vegetation cover already open locally at the beginning of HP3 in this lake depression (Testé 2020). Forest loss in relation to agrarian practices and settlements by the ancient Maya has been described regionally for this period (Anselmetti et al. 2007; Dunning et al. 1998; Islebe et al. 1996; Jones 1991; Leyden 2002; Leyden et al. 1998; Pohl et al. 1996; Rosenmeier et al. 2002b; Testé 2020; Wahl et al. 2006, 2013). The lacustrine transgression that occurred around 1500 BCE may have resulted from anthropogenic forcing. The hydrologic budget may have been significantly modified by a decrease in evapotranspiration and soil moisture, caused by deforestation and increased soil sealing. Human impacts may have increased runoff into the watershed and groundwater inflow into the lake depression. The same processes may have increased the transfer of chemical weathering products (particularly calcium). Land use change could also have modified the biogeochemical conditions of the lake (notably via the pH), increasing turbidity and the availability of nutrients in the water. All of these changes may have led to increased carbonate precipitation (Verrecchia 2002). The rise in the level of Lake Salpetén and the  $\delta^{18}$ O minima observed shortly after ~ 1500 BCE (high level between 1550 BCE and 150 CE) are also interpreted as resulting from such anthropogenic forcing (Rosenmeier et al. 2016, 2002a, 2002b). Secondly, the ~710 - ~440 BCE hydrological episode is interpreted as a response to the anthropogenic forcing described above, coupled with a forcing by the regional climate becoming wetter (Douglas et

750

751

752

753

754

755

756

757

758

759

760

761

762

763

764

765

766

767

768

769

770

771

772

773

774

775

al. 2016). The multi-decadal to multi-centennial sedimentary variability identified during HP3 could be the result of climatic variability and/or fluctuating intensity of anthropogenic impacts.

778

776

777

- 5.2.2.1.2 Erosion and sediment transfer period 3 ( $\sim$ 1500  $\sim$ 100 BCE)
- 780 From ~1500 to ~850 BCE (ESTP3a), colluviation was strong in the margins of the lake depression (Co4 781 and possibly Co5 of E2" of CS1-S2C, Figs 4 and 11), while alluviation increased in the centre of the 782 lake basin (upper AR<sub>2</sub> and AR<sub>3</sub>, Figs 9 and 11). From ~850 to ~100 BCE (ESTP3b), a strong alluviation in 783 the centre and the margins of the lake depression (AR<sub>3-max</sub>), accompanied by the continuation of 784 colluviation (Co3 and Co2), gave this last period a high intensity of erosion and sediment transfer. 785 The ESTP2/ESTP3 transition was controlled by anthropogenic impacts, as described for HP3. ESTP3 786 therefore corresponds to the first main episode of Maya clay deposition. In the SMLs EIR, the episode 787 of increased morpho-sedimentary dynamics (ESTP3a) was contemporaneous with a period marked 788 by the first or increased forest clearing, between 2000-1000 BCE (see HP3). The peak of erosion and 789 sediment transfer (ESTP3b) was contemporary with the highest sedimentation rates of the second 790 half of the Holocene, estimated during the first millennium BCE in Lake Salpetén (Rosenmeier et al. 791 2002a), Lake Petén Itzá (Mueller et al. 2009) and Lake Laguna Yaloch (Wahl et al. 2013), and with the 792 deposit of the three oldest thick Maya clay layers in Laguna Tuspan (Fleury et al. 2015). ESTP3b was 793 probably a response to a combined anthropogenic and climatic forcing, as it was contemporary with 794 the cultivation of these lake depression margins (E2A of CS2-S10, Figs 4 and 6), the earliest 795 settlements of the Naachtun centre attested to the 4th c. BCE (Nondédéo et al. in press, 2020a), and 796 a wetter regional climate period (Douglas et al. 2016).
- 797 5.2.2.2 Period ~300/100 BCE ~200/250 CE
- 798 5.2.2.2.1 Hydrological period 4 (~ 300 BCE ~250 CE)
- HP4 was characterised by a regressive sequence and low lake levels, revealed by the lithofacies E2C of CS2-S1, E2A and E1B of CS2-S10 and E2A of SC1-S2C (Figs 6, 7, 8, 11), the low  $AR_{CaCO3}$  of  $AR_4$  relative to those of  $AR_3$  and  $AR_5$  (Figs 9 and 11) and by a phase of pedogenesis (palaeosoils Sa and Sa',

Fig. 3). From HP4 onwards, the basin margins previously located near lakeshore environments evolved durably towards relatively dewatered environments favourable to cultivation, especially maize (E2A of CS2-S10, Fig. 6). As a result, the surface area and the water volume of this intermittent lake were lower than previously.

HP4 occurred during the wettest and least drought-affected climatic period of ancient Maya history (Douglas et al. 2016). Regional climatic conditions were only drier during the late HP4 (150-250 CE) (Kennett et al. 2012), which may be recorded in the anthracological sequence of Naachtun (Dussol et al. 2021). The forcing of HP4 appears to have been mainly anthropogenic and transformed the lake hydrosystem. The sediment infill of the lake basin during ESTP3 could have reduced its storage capacity and reduced inputs from ground water run-off, as described elsewhere in the SMLs (Beach et al. 2003; Dunning et al. 2002). Maya clays probably served as aquiclude or aquitard. Moreover, the hydrologic budget of the lake basin may have been impacted by the artificial increase in water storage in reservoirs and slope soils, through the construction of hydraulic and agrarian facilities, as seen in CS1-TER1 section (Fig. 4) and the watershed (Figs 1 and 10) (Canuto et al. 2018; Castanet et al. 2019, 2021), as well as by increased water withdrawal from the lake by the ancient Maya. Another hypothesis is that a decrease in anthropogenic impacts on the biophysical environment may also have led to a decrease in the hydrological budget. This hypothesis, however, is not supported by archaeological and palaeoecological data from this watershed.

#### 5.2.2.2.2 Erosion and sediment transfer period 4 (100 BCE – $\sim$ 200/250 CE)

ESTP4 was characterised by the absence of coarse colluviation and weak alluviation ( $AR_4$ , Figs 9 and 11). It could be the result of temporary abandonment of land. In this region of the SMLs, the capital El Mirador reached its height around 150 BCE and was abandoned between 150 and 200 CE, during the end of the Late Preclassic (Hansen 1998; Wahl et al. 2014). ESTP4 could more likely result from reduced sediment connectivity between different compartments of the watershed. This would be a

response to the increase of hydraulic and agricultural structures and residential settlements in the watershed and, to the reduced sediment volume on the hillslopes since ESTP3.

828 5.2.2.3 Period ~200/250 CE -~1000/1150 CE

- 829 5.2.2.3.1 Hydrological period 5 ( $\sim$ 250 CE  $\sim$  1000 CE)
- HP5 was characterised by a return to higher lake levels (lithofacies of E2B in CS2-S1 and E1B in CS1-S2C (Figs 3, 4, 7, 8, 11). Nevertheless, the lake surface was smaller than during HP3 (Figs 10 and 11). This was probably also the case for its volume. Following the dry regional climate episode between 150 and 250 CE, HP5 benefited from relatively wetter conditions during the Classic period, particularly between 600 and 730 CE (Douglas et al. 2016; Kennett et al. 2012; Wahl et al. 2014). The climate forcing of HP5 was coupled with anthropogenic forcing related to the development of the
- 5.2.2.3.2 Erosion and sediment transfer period 5 ( $\sim$ 200/250 CE  $\sim$ 1150 CE)

Naachtun city, through processes comparable to those proposed during HP3.

ESTP5, characterised by increased alluviation (AR5), was coupled with coarse colluviation (Co1) around ~250-400 CE (Figs 4, 9, 11). The latter occurred during the height of the city's monumental construction (Hiquet et al. in press). The erosion of the *bajo* hillslope was probably a consequence. Alluviation increased and AR<sub>MM</sub> were the highest in the last five millennia, between ~500 and ~1000 CE. The intensity of erosion and sediment transfer was higher during ESTP5 than ESTP3. This intensity is explained by the impacts of an increasing population, particularly during the population peak identified in the city of Naachtun by Hiquet (2020) beetwen 750 and 950 CE. Indeed, in the watershed, archaeological and geoarchaeological surveys [LiDAR remote sensing and field work, (Castanet et al. 2019; Nondédéo et al. 2020b)] revealed an average density of 150 residential structures per km² (24/km² for the Preclassic and 126/km² for the Classic), 1.6% of the surface developed as platforms of monumental and residential place or of patio group, 1.13% of the surface developed as quarries (density: 127.1/km²), an average of 2.9 km of agricultural terraces per km² and

- 99 water reservoirs (density: 5.7/km²) (Figs 1D and 1E). ESTP5 corresponds to the second main episode of Maya clay deposition.
- 852 *5.2.3 Final- and post-anthropogenic baseline of hydro-sedimentary dynamics under the control of*
- 853 the climate and Maya legacies, ~1000/1150 CE to Present
- 854 5.2.3.1 Hydrological period 6: from  $\sim 1000$  CE to  $\sim 1300$  CE
- HP6 probably saw the succession of a short episode of lowering of the lake level (HP6a) between \*\*1000 +/- 70 and \*\*1150 +/- 70 CE (Early Postclassic), followed by a short episode of lake level rise in the Postclassic (HP6b), between \*\*1150 +/- 70 and \*\*1300 +/- 70 CE (E2A1 and E2A2 of CS2-S1, Figs 7 and 11). HP6a may represent a response to the great drought phase described during the 11<sup>th</sup> century CE (Kennett et al. 2012). HP6b may have been a response to wetter conditions described during the 12<sup>th</sup> and 13<sup>th</sup> centuries CE. Anthropogenic forcing of HP6 is not retained, as the

archaeological data do not show short successive periods of land use changes.

5.2.3.2. Hydrological period 7: from  $\sim$  1300 to present.

861

869

870

871

872

873

874

- HP7 was characterised by the continuous decline of the lake levels (E1 of CS2-S1, Figs 7, 9, 11), beginning during the HP5/HP6 transition. The desertion of the region by the populations (Dussol et al. 2019) and drier climatic conditions identified regionally from the 14<sup>th</sup> to the 18<sup>th</sup> century (Haug et al. 2001; Hodell et al. 2005b; Kennett et al. 2012) may have induced this sustained decline in the hydrologic budget of the intermittent lake.
- 5.2.3.3 Erosion and sediment transfer period 6: from ~1150 CE to Present.
  - The lack of colluviation and lower alluviation in this period compared to ESTP5 and ESTP3b (Figs 9 and 11) result from the abandonment of the city of Naachtun (Nondédéo et al. 2020a) and forest regrowth (Testé 2020). This is comparable to the decrease in sedimentation rates observed in the Yaloch Laguna (Wahl et al. 2013) and Lake Salpetén (Anselmetti et al. 2007). These facts attest to the end of Maya clay deposition in the SMLs. Nevertheless, within the El Infierno *bajo* lake depression, AR<sub>MM</sub> are 1.5 to 3 times the pre-anthropic reference values (ESTP2). This could indicate that despite

the permanent abandonment of the centre of Naachtun, human settlements may have persisted in the watershed. Moreover, it could demonstrate that in terms of alluviation, the complete cessation of anthropogenic impacts for a millennium did not allow a return to conditions similar to preanthropic conditions.

- 5.3 Implications of past hydro-sedimentary dynamics for the history of anthropization and variations in water and soil resources.
- 5.3.1 A very long period of occupation and land use in the bajos (lowlands) and hilly areas(uplands) of the Southern Maya Lowlands EIR.

By documenting the first major anthropogenic impacts on hydro-sedimentary dynamics as early as ~ 1500 BCE (ESTP3 and HP3, Fig. 11), our study demonstrates early human settlement in the margins of this *bajo*. This begins at the same time as neighbouring occupations in the Mirador region (including Nakbe), dated to 1400 BCE (Hansen 1991, 1998; Wahl et al. 2014) and more distant occupations in the Lake Salpetén basin (Rosenmeier et al. 2002a). This study supports the early occupation of the SMLs by farmer communities (as *bajo* communities, Kunen et al. 2000) and clarifies its temporal and spatial extension, from at least ~1500 BCE onwards, into the centre of the EIR.

The period of high-intensity erosion and sediment transfer (ESTP3b), identified between ~850 and 100 BCE, may have resulted from increased forest clearing, agriculture, soil and subsoil exploitation (quarrying). It could testify to a first population peak in this watershed. According to this interpretation, colluviation but also alluviation suggest that settlements were not only distributed along the edges of the *bajo* but also in the hilly area. These environmental responses have been contemporaneous with the emergence of the political centre of Kunal (located 4.5 km east-southeast of this *bajo*) in the Middle Preclassic (Nondédéo et al. in press, 2020a). Several Preclassic secondary centres (El Hospital, Sarraguate) and settlement structures have been identified in the studied watershed (Figs 1 and 10) and in the micro-region (Nondédéo et al. 2020b). This period of increased erosion and sediment transfer (ESTP2b) has been almost contemporaneous with the building of the

capitals of Nakbe and then of El Mirador (Hansen 1991, 1998), located between 15 and 20 km west-southwest of Naachtun. It has been also contemporaneous with the emergence of the cities of Calakmul (Folan et al. 2001) and Yaxnohcah (Anaya Hernández et al. 2017), located between 15 and 30 km further north. This study suggests that the urban development initiated between 900 and 600 BCE in this sector of the EIR covering more than 1500 km², was supported by a relatively dense regional occupation of the hinterlands and an increased exploitation of their resources. It also suggests that this evolution had major and irreversible environmental consequences, transforming morpho-sedimentary systems and hydrosystems on a large scale in the SMLs.

The decline in erosion and sediment transfer intensity, between 100 BCE and ~200/250 CE, leads us to examine two hypotheses. The first refers to a decrease in the population of the study area, corresponding to a regional demographic decline and cultural transition observed in the EIR between 100 and 250 CE (Dunning et al. 2013a, 2013b; Hansen 2013). This hypothesis is not supported in the study area, given the available archaeological (Hiquet 2020; Nondédéo et al. 2020a) and palaeoecological data (Castanet et al. 2021; Dussol et al. 2021; Testé 2020). The second involves a decrease in sedimentary connectivity under anthropogenic control, in relation to water and soil resources management.

The second and main period of high-intensity erosion and sediment transfer (ESTP5) occurred between ~200/250 CE and ~1150 CE, in response to the increased exploitation of resources (water, soil, subsoil, wood, crops). The latter was linked to the rise of the monumental epicentre of Naachtun and to population growth during the Classic period, which led to the second demographic peak around 800-830 CE, before its abandonment in the Terminal Classic period (Fig. 11) (Hiquet 2020; Nondédéo et al. 2020a, 2021). This abandonment was contemporaneous with that of many other Maya Lowland cities between ~750 and 1050 CE (Aimers 2007).

The continuation of relatively high levels of alluviation during the Postclassic (ESTP6) may be the result of the persistence of reduced human occupation following the abandonment of the city. These

observations support the thesis of the persistence of sporadic human occupation in the SMLs EIR, based on direct (archaeological) and indirect (geoarchaeological and palaeoecological) evidence, as shown at Naachtun during the Early Postclassic (950-1150 CE) (Dussol et al. 2019), in the Paixban lake basin until the arrival of Europeans (Wahl et al. 2016) and at Joyanca (Carozza et al. 2007).

During the last 5.5 millennia,  $AR_{CaCO3}/AR_{SiAl+ox}$  ratio values significantly increased and peaked between ~1500 BCE and ~1200 CE, irrespective of the HP and ESTP. We propose that this shift of the ratio results from the response of the hydrosystem and the morpho-sedimentary system to anthropogenic impacts (particularly to the openness of the forest in relation to agrarian practices and settlements), according to the processes mentioned above (see § 5.2.2.2.1.1).

### 5.3.2 Variations in water and soil resources and the resulting risks for ancient Maya

The regional hydromorphological characteristics of the El Infierno *bajo* (lake water stock, wetland, soils) made it particularly and durably attractive to the Maya. The lake in this *bajo* was intermittent most of the time (seasonal) but also alternatively perennial or dewatered during certain periods. Under climatic and/or anthropic control, water and soil resources varied quantitatively and qualitatively.

The Maya clays of the *bajo* were deposited in a polyphased process. Erosion and sediment transfer, which increased under anthropogenic control from ~1500 BCE, peaked from ~850 to ~100 BCE, under the dual control of increased human impacts and a wetter climate. Subsequently, sediment connectivity was probably reduced, presumably as a result of hydraulic and agricultural facilities, possibly since ~100 BCE. This would suggest the loss of correlation between population density, soil erosion intensity and sediment supply in the lowlands. This is described in the SMLs for the Preclassic - Classic transition and during the Classic period in response to changes in forest clearance and agriculture and/or the construction of agrarian and hydraulic structures (Anselmetti et al. 2007; Dunning et al. 1997, 2002, 2019; Wahl et al. 2013). Nevertheless, the human impacts were so strong

in the centre of Naachtun and its hinterland during the Classic that a second ESTP occurred between ~200/250 and ~1150 CE.

949

950

951

952

953

954

955

956

957

958

959

960

961

962

963

964

965

966

967

968

969

970

971

972

973

This study shows that the clay sedimentary stock was mostly constituted before the first anthropogenic impacts, except in the lake basin and the bajo margins. Significant colluvial and alluvial detrital inputs, resulting from the anthropogenic erosion on the uplands, were deposited on the bajo margins and in lakes, as described in the EIR of the SMLs (Dunning et al. 2019; Hodell et al. 2006). The Maya clays infill of this shallow lake have transformed its hydrosystem and impacted its dynamics. It likely served as an aquiclude or aquitard stopping or reducing inputs from ground water run-off, as described elsewhere in the SMLs (Beach et al. 2003; Dunning et al. 2002). In the centre of the El Infierno bajo, the top of the pre-anthropogenic clay stock was modified by the Maya for hydraulic and agrarian purposes, by creating reservoirs, canals, ditches, raised fields and drained fields (Castanet 2019; Castanet et al. 2020). Within the bajo, the diversity of Maya clays and geomorphological and hydrological contexts gave rise to a mosaic of soils. Their agronomic properties were known and exploited for agrarian purposes by the ancient Maya (Beach et al. 2008; Dunning et al. 2002; Jensen et al. 2007). The bajo soils outside the lake basin did not experience long seasonal flooding by lake overflow, but were constrained by waterlogging and desiccation. This helps to explain evidence of land use in the bajo for agrarian purposes, through drainage and irrigation techniques (the wetland features) (Castanet 2019; Castanet et al. 2020). This reinforces the thesis that the hydrological and edaphic conditions of the bajos are compatible with traditional Maya agriculture (Beach et al. 2003; Culbert et al. 1996, 1989; Dunning et al. 2002; Kunen et al. 2000). The numerous wetland features identified in the bajos of the Naachtun hinterland could constitute the palimpsest of an agrarian landscape, built and shaped over a period of 2500 years (1500 BCE-1150 CE) (Castanet et al. 2021). This could also be the case at the scale of the EIR of the SMLs. This palimpsest is currently studied in the Naachtun exploitation territory, which will allow the nature and dynamics of the socio-ecosystem to be analysed (Castanet et al. 2021).

Changes in hydrology, erosion and sediment transfer had agronomic and economic implications. The earliest peak of AR<sub>MM</sub> (from ~850 to ~100 BCE) is indicative of a period of high soil erosion in the hilly area. Management of the induced edaphic and agronomic risks most likely led to an increase in agricultural terracing on the uplands during this period, as was the case elsewhere in the SMLs, where soil conservation features were constructed as early as ~ 550 BCE (Middle Preclassic) and then mostly between 250 and 850 CE (Classic) (Beach 1998; Beach et al. 2002, 2003; Dunning et al. 2002). Nevertheless, soils developed with eroded material deposited on the margins of the El Infierno bajo, constituted an edaphic resource, exploited from the Late Preclassic onwards for maize cultivation, in the ancient perennial wetland of this bajo, and more broadly in the bajos zone of the EIR (Dunning et al. 2019). These results support the thesis that, as urbanism took hold in the region from ~800 BCE, 'the bajo zone in the EIR became the heartland of Preclassic Maya civilization' (Dunning et al. 2019). Moreover, marked environmental transformations, resulting from resource exploitation for more than 1500 years during the Preclassic period, did not prevent the development and influence of this Maya regional capital in the same geographical space and during another millennium. Subsequently, the episode of low lake level identified between ~1000 +/- 70 and ~1150 +/- 70 CE (Early Postclassic) could only have reduced agricultural yields in relation to previous periods, during the demographic peak of the Late Classic. Furthermore, it may have increased socio-environmental, economic and political tensions in the socio-ecosystem, shortly before and at the same time as the abandonment of Naachtun. These interactions are comparable to those experienced by many other SMLs cities, between 750 and 950 CE (Kennett et al. 2012; Lentz et al. 2014; Turner and Sabloff 2012). Lastly, several factors could explain the continuation of alluviation with strong AR<sub>MM</sub> after 1150 CE

974

975

976

977

978

979

980

981

982

983

984

985

986

987

988

989

990

991

992

993

994

995

996

997

998

999

(during the Postclassic). This could be a response to continuing anthropogenic impacts during the Postclassic. It could also indicate a significant recovery of sediment connectivity and thus the very slow readjustment of the morpho-sedimentary system after the complete removal of anthropogenic impacts. Indeed, the reduction in connectivity during the Preclassic and Classic periods resulted in the storage of eroded or artificially displaced sediment on the slopes. Furthermore, the conditions of

low pre-anthropogenic denudation (nature of soils and/or forest) might not have been recovered after more than 2500 years of strong anthropogenic impacts. According to this hypothesis, anthropogenic forcing would have induced the crossing of an irreversible threshold in the nature and dynamics of this hydrosystem and this morpho-sedimentary system of the EIR centre of the SMLs. In any case, the dynamics of the Maya early Anthropocene created legacies for current and future environmental dynamics.

## 6. Conclusions

This study revealed, analysed and compared the response of a hydrosystem and a morphosedimentary system, durably transformed by ancient Maya societies, to anthropogenic and climate drivers during the past 5500 years. It provides information and analyses in an integrated way on four of the five major 'golden spikes', considered by Beach et al. (2015) for the Maya early Anthropocene: "Maya Clay", the palaeosoil sequence, the soil profiles of carbon isotope ratios and indicators (quantified LiDAR derived data) of human activity (housing, terraces, wetland fields) still present in the landscape. Henceforth, the knowledge of past hydro-sedimentary fluctuations will allow for the study of their agronomic and economic implications on the dynamics and sustainability of past socioecosystems, and their current implications on the environmental dynamics of the Maya Biosphere Reserve.

## **Acknowledgements and funding**

This work was supported by the programme *Petén Norte NAACHTUN* (2010-2022, dir. P. Nondédéo, supports: MEAE, CNRS, *Université Paris 1 Panthéon-Sorbonne*, *Pacunam* foundation, *Perenco* company, *Simone et Cino Del Duca* foundation), by the project *MAYANAT* (2020-2021, coord. C. Castanet, supports: CNRS INEE) and the project *HYDROAGRO* (2014-2016, coord. E. Lemonnier, C. Castanet, supports: *Université Paris 1 Panthéon-Sorbonne*). Financial support from the *LabEx DynamiTe* (ANR-11-LABX-0046), in the framework of the programme "*Investissements d'Avenir*". It forms part of CEMCA activities in Central America. Fieldwork was undertaken with the permission of

1026 from *Uaxactun*. 1027 References 1028 1029 Aimers, J.J., 2007. What Maya Collapse? Terminal Classic Variation in the Maya Lowlands. J Archaeol 1030 Res 15, 329–377. https://doi.org/10.1007/s10814-007-9015-x 1031 An, F., Lai, Z.P., Liu, X., Fan, Q.S., Wei, H.C., 2018. Abnormal Rb/Sr ratio in lacustrine sediments of 1032 Qaidam Basin, NE Qinghaie Tibetan Plateau: A significant role of aeolian dust input. 1033 Quaternary International 469, 44-57, http://dx.doi.org/10.1016/j.quaint.2016.12.050 1034 Anaya Hernández, A., Reese-Taylor, K., Peraumaki-Brown, M., Walker, D.S., Dunning, N.P., Flores 1035 Esquivel, A., Vázquez Lopez, V.A., Morton, S., Brewer, J., 2017. Yaxnohcah, Campeche. Un centro urbano multi-nodal del Preclásico. Paper presented at VIII Mesa Redonda de 1036 1037 Palenque. Palenque, Chiapas. 1038 Anselmetti, F., Hodell, D.A., Ariztegui, D., Brenner, M., Rosenmeier, M.F., 2007. Quantification of soil 1039 erosion rates related to ancient Maya deforestation. Geology 35, 915-918 1040 https://doi.org/10.1130/G23834A.1 1041 Bautista, F., Palacio Aponte, G., Quintana, P., Zinck, J.A., 2011. Spatial distribution and development 1042 of soils in tropical karst areas from the Peninsula of Yucatan, Mexico. Geomorphology 135, 1043 308-321. https://doi.org/10.1016/j.geomorph.2011.02.014 1044 Beach, D., Luzzadder-Beach, S., Cook, D., Krause, S., Doyle, C., Eshleman, S., Wells, G., Dunning, N., 1045 Brennan, M.-L., Brokawe, N., Cortes-Rincon, M., Hammond, G., Terry, R., Treina, D., Ward, S., 1046 2018. Stability and instability on Maya Lowlands tropical hillslope soils. Geomorphology 305, 1047 185–208. http://dx.doi.org/10.1016/j.quaint.2017.02.031 1048 Beach, T., 1998. Soil catenas, tropical deforestation, and ancient and contemporary soil erosion in 1049 the Petén, Guatemala. Physical Geography 19, 378–404. 1050 https://doi.org/10.1080/02723646.1998.10642657 Beach, T., Luzzadder-Beach, S., Cook, D., Dunning, N., Kennett, D., Krause, S., Terry, R., Trein, D., 1051 1052 Valdez, F., 2015. Ancient Maya impacts on the Earth's surface: an Early Anthropocene 1053 analog? Quat. Sci. Rev. 124, 1–30. https://doi.org/10.1016/j.quascirev.2015.05.028 1054 Beach, T., Luzzadder-Beach, S., Dunning, N., Cook, D., 2008. Human and natural impacts on fluvial and karst systems in the Maya Lowlands. Geomorphology 101, 301–331. 1055 1056 https://doi.org/10.1016/j.geomorph.2008.05.019 1057 Beach, T., Luzzadder-Beach, S., Dunning, N., Hageman, J., Lohse, J., 2002. Upland agriculture in the 1058 Maya Lowlands: ancient conservation in northwestern Belize. Geogr. Rev. 92, 372–397. 1059 https://doi.org/10.1111/j.1931-0846.2002.tb00149.x

the Instituto de Antropología e Historia (IDAEH) of Guatemala and with the assistance of workers

1025

1060 1061 1062 1063	Beach, T., Luzzadder-Beach, S., Dunning, N., Scarborough, V., 2003. Depression soils in the lowland tropics of northwestern Belize: Anthropogenic and natural origins, in: Lowland Maya Area: Three Millennia at the Human-Wildland Interface. Hawthorn Press, Binghamton, NY, pp. 139–174.
1064 1065 1066 1067	Beach, TP., Luzzadder-Beach, S., Dunning, N.P., Jones, J.G., Lohse, J.C., Guderjan, T.H., Bozarth, S., Millspaugh, S., Bhattacharya, T., 2009. A review of human and natural changes in Maya Lowlands wetlands over the Holocene. Quat. Sci. Rev. 28, 1710–1724. https://doi.org/10.1016/j.quascirev.2009.02.004
1068 1069 1070	Bhagowati, B. and Ahamad, K.U., 2019. A review on lake eutrophication dynamics and recent developments in lake modeling, Ecohydrology & Hydrobiology, 19, 155–166 https://doi.org/10.1016/j.ecohyd.2018.03.002
1071 1072	Blaauw, M., 2010. Methods and code for 'classical' age-modelling of radiocarbon sequences. Quaternary Geochronology 5, 512-518. https://doi:10.1016/j.quageo.2010.01.002
1073 1074	Blaauw, M., and Christen, JA., 2005. Radiocarbon peat chronologies and environmental change. Appl. Statist., 54, Part 4, pp. 805–816. https://doi.org/10.1111/j.1467-9876.2005.00516.x
1075 1076 1077 1078 1079	Blaauw, M., and Christen, JA., 2011. Flexible Paleoclimate Age-Depth Models Using an Autoregressive Gamma Process. Bayesian Anal. 6, 3, 457-474. https://doi:10.1214/11-ba618 Brock F., Higham T., Ditchfield P., Bronk Ramsey C. 2010, Current pretreatment methods for AMS radiocarbon dating at the Oxford Radiocarbon Accelerator Unit (ORAU), Radiocarbon, 52 103–112. https://doi.org/10.1017/S0033822200045069
1080 1081	Bronk Ramsey, C., 2008. Deposition models for chronological records. Quat. Sci. Rev. 27, 42-60. https://doi:10.1016/j.quascirev.2007.01.019
1082 1083	Bronk Ramsey, C., 2009. Bayesian analysis of radiocarbon dates. Radiocarbon 51, 337–360. https://doi.org/10.1017/S0033822200033865
1084 1085	Bullock, F., Fedoroff, N., Jongerius, A., 1985. Handbook for soil thin section description, Waine. ed. Albrighton. pp 152.
1086 1087	Campy, M., Meybeck, M., 1995. Les sédiments lacustres, in: Limnologie Générale, Collection d'écologie. Masson, Paris, pp. 6–59. ISBN 2-225-84687-1.
1088 1089 1090 1091 1092	Canuto, M.A., Estrada-Belli, F., Garrison, T.G., Houston, S.D., Acuña, M.J., Kováč, M., Marken, D., Nondédéo, P., Auld-Thomas, L., Castanet, C., Chatelain, D., Chiriboga, C.R., Drápela, T., Lieskovský, T., Tokovinine, A., Velasquez, A., Fernández-Díaz, J.C., Shrestha, R., 2018. Ancient lowland Maya complexity as revealed by airborne laser scanning of northern Guatemala. Science 361. https://doi.org/10.1126/science.aau0137
1093 1094 1095 1096	Carozza, JM., Galop, D., Métailié, JP., Vannière, B., Bossuet, G., Monna, F., Lopez-Saez, JA., Arnaud, MC., Breuil, V., Forné, M., Lemonnier, E., 2007. Landuse and soil degradation in the Southern Maya Lowlands from Pre-Classic to Post-Classic times: The case of La Joyanca (Petén, Guatemala). Geodinamica Acta 20, 195–207. https://doi.org/10.3166/ga.20.195-207

1097	Castanet, C. 2008. « La Loire en val d'Orléans. Dynamiques fluviales et socio-environnementales
1098	durant les derniers 30 000 ans : de l'hydrosystème à l'anthroposystème. » (Unpublished Ph.D
1099	thesis), Université Paris 1 Panthéon Sorbonne, Paris. pp. 585.
1100	Castanet, C., 2019. Caracterización de los "wetland features" (Operación IV.6), in: Proyecto Petén-
1101	Norte Naachtun 2015-2018, Informe Final de La Novena Temporada de Campo 2018.
1102	CNRS/Université de Paris 1/CEMCA. Informe entregado al Instituto de Antropología e Historia
1103	de Guatemala, Guatemala city, pp. 211–228.
1104	Castanet, C., Fernandes, A., Garnier, A., Testé, M., Cavero, J., Develle-Vincent, A.L., Sipos, G., Dussol,
1105	L., Purdue, L., Lemonnier, E., Nondédéo, P., 2020. Hydro-agro-system of the wetlands in the
1106	Central Maya Lowlands: land use sustainability and the joint water management (hinterland
1107	of Naachtun, Petén tropical forest, Guatemala), in: 12 <sup>th</sup> International conference on
1108	Quaternary, AFEQ-CNF INQUA-GFG, Paris-Aubervilliers.
1109	Castanet C., Nondédéo P., Dussol L., Testé M., Purdue L., Hiquet J., Lemonnier E., Garnier A., Dorison
1110	A., Tomadini N., Grouard S., Goudiaby H., Morales-aguilar C., Limondin-Lozouet N., Cavero J.,
1111	Develle-Vincent AL., Hatte C., Gauthier C., Lanos P., Mokadem F. and Sipos G., 2021. Nature
1112	et dynamique du socio-écosystème maya du territoire de subsistance de la cité de Naachtun
1113	entre 1500 BCE et 1000 CE (Petén, Guatemala), in: Proceedings of the 41st Nice Côte d'Azur
1114	International Meeting of Archaeology and History, 'Biodiversities, Environments and Societies
1115	since Prehistory: new markers and integrated approaches'. APDCA ed., Nice, pp. 153-167.
1116	ISBN: 2-904110-64-X.
1117	Castanet, C., Nondédéo, P., Lemonnier, E., Purdue, L., Dorison, A., Cuenot, J.F., Pageau, J., Hiquet, J.,
1118	Michelet, D., Begel, J., Morales-Aguilar, C., Garrido, L., 2019. El LiDAR como herramienta para
1119	un acercamiento a la gestión de los recursos naturales (agua y suelos): el caso de Naachtun,
1120	Petén, Guatemala., in: XXXII Simposio de Investigaciones Arqueológicas En Guatemala.
1121	Museo Nacional de Arqueología y Etnología de Guatemala, Guatemala, pp. 665–677.
1122	Castanet, C., Purdue, L., Lemonnier, E., Nondédéo, P., 2016. Dynamiques croisées des milieux et des
1123	sociétés dans les basses terres tropicales mayas : hydrosystème et agrosystème à Naachtun
1124	(Guatemala). Les Nouvelles de l'archéologie 142, 32–37. https://doi.org/10.4000/nda.3275
1125	Chang, H., An, Z., Wu, F., Jin, Z., Liu, W., Song, Y., 2013. A Rb/Sr record of the weathering response to
1126	environmental changes in westerly winds across the Tarim Basin in the late Miocene to the
1127	early Pleistocene. Palaeogeogr. Palaeoclimatol. Palaeoecol. 15, 364-373
1128	https://doi.org/10.1016/j.palaeo.2013.06.006
1129	Cohen, A.S., 2003. Paleolimnology: the History and Evolution of Lake Systems. Oxford University
1130	Press, Oxford. 528 p. http://dx.doi.org/10.1093/oso/9780195133530.001.0001
1131	Cooke, C.W., 1931. Why the Mayan cities of the Peten district, Guatemala, were abandoned? Journal
1132	of the Washington Academy of Sciences 21, 283–287.
1133	Cowgill, U.M., Hutchinson, G.E., 1963. El Bajo de Santa Fe. Transactions of the American Philosophica
1134	Society 53, 3-44. https://doi.org/10.2307/1005889

1135 1136 1137 1138	Culbert, T.P., Fialko, V., McKee, B., Grazioso, L., Kunen, J., 1996. Investigación arqueológica en el Bajo La Justa: la temporada de 1996, in: X Simposio de Investigaciones Arqueológicas En Guatemala. Museo Nacional de Arqueología y Etnología de Guatemala, Guatemala City, pp. 367–371.
1139 1140	Culbert, T.P., Levi, L., Cruz, L., 1989. The Rio Azul agronomy program: the 1986 season (No. 4), Adams, R.E. (Ed.), Rio Azul reports. University of Texas at San Antonio.
1141 1142 1143	Curtis, J.H., Hodell, D.A., Brenner, M., 1996. Climate variability on the Yucatan Peninsula (Mexico) during the past 3500 years, and implications for Maya cultural evolution. Quat. Res. 46, 37–47. https://doi.org/10.1006/qres.1996.0042
1144 1145	Dahlin, B.H., Dahlin, A., 1994. Platforms in the akalche at El Mirador, Peten, Guatemala and their implications. Geoarchaeology 9, 203–237. https://doi.org/10.1002/gea.3340090303
1146 1147 1148	Dasch, E.J., 1969. Strontium isotope in weathering in profiles, deep sea sediments and sedimentary rocks. Geochim. Cosmochim. Acta 33, 1521-1552. https://doi.org/10.1016/0016-7037(69)90153-7
1149 1150	Dearing, J.A., 1994. Environmental magnetic susceptibility using the Barrington MS2 System, Chi Publishing. ed. Kentworth. pp 104.
1151 1152 1153	Dearing, J.A., Hakansson, H., Liedberg-Jöhnsson, B., Persson, A., Skansjö, S., Widholm, D., El-Daoushy, S., 1987. Lake sediments used to quantify the erosional response to land use change in southern Sweden. Oïkos 50, 60–78. https://doi.org/10.2307/3565402
1154 1155	Deevey, E.S., 1978. Holocene forests and Maya disturbance near Quexil Lake, Petén, Guatemala. Polskie Archiwum Hydrobiologii 25, 117–129.
1156 1157 1158	Deevey, E.S., Gross, M.S., Hutchinson, G.E., Kraybill, H.L., 1954. The natural C-14 contents of materials from hard-water lakes. Proceedings of the National Academy of Sciences 40, 285–288. https://doi.org/10.1073/pnas.40.5.285
1159 1160 1161	Deevey, E.S., Rice, D.S., Vaughan, P.M., Brenner, M., Flannery, M.S., 1979. Mayan urbanism: Impact on a tropical karst environment. Science 206, 298–306. https://doi.org/10.1126/science.206.4416.298
1162 1163	Deines, P., 1980. The isotopic composition of reduced organic carbon, in: Hand Book of Environmental Isotope Geochemistry. Elsevier, Amsterdam, pp. 329–406.
1164 1165	de Vries H, Barendsen GW. 1954. Measurements of age by the carbon-14 technique. Nature 174:1138–41. https://doi.org/10.1038/1741138a0
1166 1167 1168	Digerfeldt, G., Sandgren, P., Olsson, S., 2007. Reconstruction of Holocene lake-level changes in Lake Xinias, central Greece. The Holocene 17, 361–367. https://doi.org/10.1177/0959683607076449
1169 1170 1171	Douglas, P.M.J., Demarest, A.A., Brenner, M., Canuto, M.A., 2016. Impacts of Climate Change on the Collapse of Lowland Maya Civilization. Annu. Rev. Earth Planet. Sci. 44, 613–645. https://doi.org/10.1146/annurev-earth-060115-012512

11/2	Douglas, P.M.J., Pagani, M., Canuto, M.A., Brenner, M., Hodell, D.A., Eglinton, T.I., Curtis, J.H., 2015.
1173	Drought, agricultural adaptation, and sociopolitical collapse in the Maya Lowlands. Proc. Natl
1174	Acad. Sci. 112, 5607–5612. https://doi.org/10.1073/pnas.1419133112
1175	Dunning, N., Beach, T., 1994. Soil erosion, slope management, and ancient terracing in the Maya
1176	Lowlands. Latin American Antiquity 5, 51–69. https://doi.org/10.2307/971902
1177	Dunning, N., Beach, T., Rue, D.J., 1997. The paleoecology and ancient settlement of the Petexbatun
1178	region, Guatemala. Ancient Mesoamerica 8, 255–266.
1179	https://doi.org/10.1017/S0956536100001711
1180	Dunning, N., Hernández, A.A., Beach, T., Carr, C., Griffin, R., Jones, J.G., Lentz, D.L., Luzzadder-Beach,
1181	S., Reese-Taylor, K., Šprajc, I., 2019. Margin for error: Anthropogenic geomorphology of Bajo
1182	edges in the Maya Lowlands. Geomorphology 331, 127–145.
1183	https://doi.org/10.1016/j.geomorph.2018.09.002
1184	Dunning, N.P., Beach, T., Luzzadder-Beach, S., 2012. Kax and kol: collapse and resilience in Lowland
1185	Maya Civilization. Proc. Natl. Acad. Sci. 109, 3652–3657.
1186	https://doi.org/10.1073/pnas.1114838109
1187	Dunning, N.P., Beach, TP., Grasiozo Sierra, L., Jones, J.G., Lentz, D.L., Luzzadder-Beach, S.,
1188	Scarborough, V.L., Smyth, M.P., 2013a. A Tale of Two Collapses: environmental variability and
1189	cultural disruption in the Maya Lowlands. Diálogo Andino - Revista de Historia, Geografía y
1190	Cultura Andina 41, 171–183. http://dx.doi.org/10.4067/S0719-26812013000100011
1191	Dunning, N.P., Luzzadder-Beach, S., Beach, T., Jones, J.G., Scarborough, V.L., Culbert, T.P., 2002.
1192	Arising from the bajos: the evolution of a Neotropical landscape and the rise of Maya
1193	Civilization. Ann. Assoc. Am. Geogr. 92, 267–282. https://doi.org/10.1111/1467-8306.00290D
1194	Dunning, N.P., Rue, D.J., Beach, T., Covich, A., Traverse, A., 1998. Human–environment interactions in
1195	a tropical watershed: the paleoecology of Laguna Tamarindito, El Peten, Guatemala. Journal
1196	of Field Archaeology 25, 139–151. https://doi.org/10.1179/009346998792005487
1197	Dunning, N.P., Wahl, D., Beach, T., Jones, J.G., Luzzadder-Beach, S., Mc Cane, C., 2013b. The End of
1198	the Beginning. Drought, Environmental Change, and the Preclassic to Classic Transition in the
1199	East-Central Maya Lowlands, in: The Great Maya Droughts in Cultural Context. Case Studies
1200	in Resilience and Vulnerability. Boulder: University Press of Colorado, pp. 107–126.
1201	Dussol, L., Elliot, M., Michelet, D., Nondédéo, P., 2021. Fuel economy, woodland management and
1202	adaptation strategies in a Classic Maya city: applying anthracology to urban settings in high
1203	biodiversity tropical forests. Vegetation History and Archaeobotany, 30, 175–192.
1204	https://doi.org/10.1007/s00334-020-00776-0
1205	Dussol, L., Sion, J., Nondédéo, P., 2019. Late fire ceremonies and abandonment behaviors at the
1206	Classic Maya city of Naachtun, Guatemala. Journal of Anthropological Archaeology 56,
1207	101099. https://doi.org/10.1016/j.jaa.2019.101099

1208 1209 1210	tropical Atlantic and Pacific Oceans. J. Clim. 12, 2093–2103. https://doi.org/10.1175/1520-0442(1999)012<2093:TDOCRO>2.0.CO;2
1211 1212 1213 1214	Enters, D., Kirilova, E., Lotter, A.F., Lücke, A., Parplies, J., Jahns, S., Kuhn, G., Zolitschka, B., 2010. Climate change and human impact at Sacrower See (NE Germany) during the past 13,000 years: a geochemical record, J Paleolimnol, 43:719–737 https://doi.org/10.1007/s10933-009-9362-3
1215 1216 1217	Farquhar, G.D., O'Leary, M.H., Berry, J.A., 1982. On the relationship between carbon isotope discrimination and the intercellular carbon dioxide concentration in leaves. Australian Journal of Plant Physiology 9, 121–137. https://doi.org/10.1071/PP9820121
1218 1219 1220	Fernandez-Diaz, J.C., Carter, W.E., Glennie, C., Shrestha, R.L., Pan, Z., Ekhtari, N., Singhania, A., Hauser, D., Sartori, M., 2016. Capability assessment and performance metrics for the Titan multispectral mapping lidar. Remote Sensing 8, 936. https://doi.org/10.3390/rs8110936
1221 1222 1223 1224	Fleury, S., Malaize, B., Giraudeau, J., Galop, D., Bout-Roumazeilles, V., Martinez, P., Charlier, K., Carbonel, P., Arnauld, M.C., 2015. Reprint of: Impacts of Mayan land use on Laguna Tuspan watershed (Petén, Guatemala) as seen through clay and ostracode analysis. Journal of Archaeological Science 54, 410–420. https://doi.org/10.1016/j.jas.2014.05.032
1225 1226 1227	Folan, W.J., Fletcher, L.A., Hau, J.M., Florey, L., 2001. Las Ruinas de Calakmul, Campeche, México: Un lugar central y su paisaje cultural. (No. Appendices A–C.). Centro de Investigaciones Históricas y Sociales, Universidad Autónoma de Campeche, Campeche, Mexico.
1228 1229	Ford, D.C. and Williams, P., 2007. Karst Hydrogeology and Geomorphology. John Wiley, Chichester, pp. 562. https://doi.org/10.1002/9781118684986
1230 1231	Freytet, P., Verrecchia, E.P., 2002. Lacustrine and palustrine carbonate petrography: an overview. Journal of Paleolimnology 27, 221–237. https://doi.org/10.1023/A:1014263722766
1232 1233	Gaillard, J.F. 1995, Limnologie chimique : principes et processus, in: Limnologie Générale, Collection d'écologie. Masson, Paris, 115-156. ISBN 2-225-84687-1.
1234	García, E., 1990. "Climas", 1: 4000 000. IV.4.10 (A). Atlas Nacional de México. Vol. II.
1235 1236	García, E., 1981. Modificaciones al Sistema de Clasificación Cli-mática de Koeppen para Adaptarlo a las Condiciones de la República Mexicana., Offset Larios. ed. México.
1237 1238 1239	Giannini, A., Kushnir, Y., Cane, M.A., 2000. Interannual variability of Caribbean rainfall, ENSO, and the Atlantic Ocean. J. Clim. 13, 297–311. https://doi.org/10.1175/1520-0442(2000)013<0297:IVOCRE>2.0.CO;2
1240 1241 1242	Green, P.J., and Silverman, B.W., 1994. Nonparametric regression and generalized linear models, a roughness penalty approach. Monographs on Statistics and Applied Probability, 58, Chapman & Hall, London, pp 182.
1243 1244	Hale, M.E., 1984. The lichen line and high water levels in a freshwater stream in Florida. The bryologist 87, 261–265. https://doi.org/10.2307/3242807

1245	Hansen, 1991, 1991. The road to Nakbe. Natural History 5, 8–14.
1246 1247 1248	Hansen, R.D., 2013. The beginning of the End: Conspicuous Consumption and Environmental Impact of the Preclassic Lowland Maya, in: An Archaeological Legacy, Essays in Honor of Ray T. Matheny. Provo: The University of Utah Press, pp. 241–285.
1249 1250 1251	Hansen, R.D., 1998. Continuity and Disjunction: The Pre-Classic Antecedents of Classic Maya Architecture., in: Function and Meaning in Classic Maya Architecture. Dumbarton Oaks, Washington, pp. 49–122.
1252 1253	Hansen, R.D., 1990. Excavations in the tigre complex El Mirador, Petén, Guatemala., Provo, Utah.  Brigham Young University. ed, Papers of the New World Archaeological Foundation.
1254 1255 1256	Haslett, J., and Parnell, A., 2008. A simple monotone process with application to radiocarbon-dated depth chronologies. Appl. Statist., 57, Part 4, pp. 399–418. https://doi.org/10.1111/j.1467-9876.2008.00623.x
1257 1258 1259	Haug, G.H., Hughen, K.A., Sigman, D.M., Peterson, L.C., Rohl, U., 2001. Southward migration of the intertropical convergence zone through the Holocene. Science 293, 1304–8. https://doi.org/10.1126/science.1059725
1260 1261 1262 1263	Heymann, C., Nelle, O., Dörfler, W., Zagana, H., Nowaczyk, N., Xue, J., Unkel, I., 2013. Late Glacial to mid-Holocene palaeoclimate development of Southern Greece inferred from the sediment sequence of Lake Stymphalia (NE-Peloponnese). Quaternary International 302, 42-60, http://dx.doi.org/10.1016/j.quaint.2013.02.014
1264 1265 1266	Hiquet, J., 2020. Essor monumental et dynamiques des populations. Le cas de la cité de Naachtun (Guatemala) au Classique ancient (150-550 apr. JC.). (Unpublished Ph.D thesis). Université Paris 1 Panthéon-Sorbonne, Paris.
1267 1268 1269 1270	Hiquet, J., Castanet, C., Dussol, L., Nondédéo, P., Testé, M., Purdue, L., Tomadini, N., Grouard, S., Dorison, A. ( <i>in press</i> ), After the Preclassic Collapse. A socio-environmental contextualization of the rise of Naachtun (Guatemala), in: <i>Shaping Cultural Landscapes: Connecting Agriculture, Crafts, Construction, Transport, and Resilience Strategies</i> . Sidestone Press, Leiden.
1271 1272 1273	Hodell, D., Anselmetti, F., Brenner, M., Ariztegui, D., and the PISDP Scientific Party, 2006. The Lake Petén Itzá Scientific Drilling Project, Sci. Dril., 3, 25–29 https://doi.org/10.2204/iodp.sd.3.02.2006
1274 1275 1276	Hodell, D.A., Brenner, M., Curtis, J.H., 2005a; Terminal Classic drought in the northern Maya lowlands inferred from multiple sediment cores in Lake Chichancanab (Mexico). Quaternary Science Reviews, 24, 1413–1427, https://doi.org/10.1016/j.quascirev.2004.10.013
1277 1278 1279	Hodell, D.A., Brenner, M., Curtis, J.H., Medina-Gonzalez, R., Can, E.I.C., Albornaz-Pat, A., Guilderson, T.P., 2005b. Climate change on the Yucatan Peninsula during the Little Ice Age. Quat. Res. 63, 109–121. https://doi.org/10.1016/j.yqres.2004.11.004
1280 1281	Hodell, D.A., Curtis, J.H., Brennert, M., 1995. Possible role of climate in the collapse of Classic Maya Civilization. Nature 375. https://doi.org/10.1038/375391a0

1282 1283 1284	1991. Reconstruction of Caribbean climate change over the past 10,500 years. Nature 352, 790–793. https://doi.org/10.1038/352790a0
1285 1286 1287 1288	Huber, R., Ismail-Meyer, K., 2012. Cham-Eslen (Kanton Zug, Schweiz): ein jungneolithisches Haus mit (fast) allem Drum und Dran? Taphonomische Aspekte einer Seeufersiedlung, in: Taphonomische Forschungen (Nicht Nur) Zum Neolithikum. Fokus Jungsteinzeit 3. Welt und Erde Verlag, Kerpen-Loogh, pp. 83–106.
1289 1290 1291	Hussein, J., Adey, M.A., 1998. Changes in microstructure, voids and b-fabric of surface samples of a Vertisol caused by wet/dry cycles. Geoderma 85, 63–82. https://doi.org/10.1016/S0016-7061(98)00014-7
1292	Instituto Geographico Nacional, 1970. Mapa Geologico de la Republica de Guatemala.
1293 1294 1295	Islebe, G.A., Hooghiemstra, H., Brenner, M., Curtis, J.H., Hodell, D.A., 1996. A Holocene vegetation history from lowland Guatemala. The Holocene 6, 265–271. https://doi.org/10.1177/095968369600600302
1296 1297 1298 1299	Jensen, C.T., Moriarty, M.D., Johnson, K.D., Terry, R.E., Emery, K.F., Sheldon, N.D., 2007. Soil Resources of the Motul De San José Maya: Correlating Soil Taxonomy and Modern Itzá Maya Soil Classification Within a Classic Maya Archaeological Zone. Geoarcheology: An International Journal 22, 337–357. https://doi.org/doi:10.1002/gea.20156
1300 1301 1302	Jin, Z., Cao, J., Wu, J., Wang, S., 2006. A Rb/Sr record of catchment weathering response to Holocene climate change in Inner Mongolia. Earth Surf. Process. Landforms 31, 285–291. https://doi.org/10.1002/esp.1243
1303 1304	Jones, J.G., 1991. Pollen Evidence of Prehistoric Forest Modification and Maya Cultivation in Belize.  Department of Anthropology. Texas A&M, College Station.
1305 1306 1307	Kennett, DJ., Beach, TP., 2013. Archeological and environmental lessons for the Anthropocene from the Classic Maya collapse. Anthropocene 4, 88–100. https://doi.org/10.1016/j.ancene.2013.12.002
1308 1309 1310 1311 1312	<ul> <li>Kennett, D.J., Breienbach, S.F.M., Aquino, V.V., Asmerom, Y., Awe, J., Baldini, J.U.L., Bartlein, P.,</li> <li>Culleton, B.J., Ebert, C., Jazwa, C., Macri, M.J., Marwan, N., Polyak, V., Prufer, K.M., Ridley,</li> <li>H.E., Sodemann, H., Winterhalder, B., Haug, G.H., 2012. Development and disintegration of</li> <li>Maya political systems in response to climate change. Science 338, 788–791.</li> <li>https://doi.org/10.1126/science.1226299</li> </ul>
1313 1314	Krishnamurthy, R.V., DeNiro, M.J., Pant, R.K., 1982. Isotope evidence for Pleistocene climatic changes in Kasmir, India. Nature 298, 640–641. https://doi.org/10.1038/298640a0
1315 1316 1317 1318	Koinig, K.A., Shotyk, W., Lotter, A.F., Ohlendorf, C., Sturm, M., 2003. 9000 years of geochemical evolution of lithogenic major and trace elements in the sediment of an alpine lake – the role of climate, vegetation, and land-use history. Journal of Paleolimnology 30, 307–320. https://doi.org/10.1023/A:1026080712312

1319 1320	the central Petén. Culture & Agriculture 22, 15–31. https://doi.org/10.1525/cag.2000.22.3.15
1321 1322 1323	Lanos, Ph., 2004. Bayesian Inference of Calibration Curves: Application to Archaeomagnetism. In: Tools for Constructing Chronologies. Crossing disciplinary boundaries. Springer-Verlag London, pp 43-82. https://doi.org/10.1007/978-1-4471-0231-1_3
1324 1325 1326	Lanos, Ph. and Dufresne, Ph., 2019a. Chronomodel version 2.0: Software for Chronological Modelling of Archaeological Data using Bayesian Statistics. Available from: http://www.chronomodel.com
1327 1328	Lanos, Ph. and Dufresne, Ph., 2019b. ChronoModel version 2.0: User manual. Available from: http://www.chronomodel.com
1329 1330 1331	Lanos, P. and Philippe, A., 2017. Hierarchical Bayesian modeling for combining dates in archaeological context. Journal de la Société Française de Statistique, 158(2): 72–88. https://hal.archives-ouvertes.fr/insu-01451371
1332 1333 1334	Lanos, P. and Philippe, A., 2018. Event date model: a robust Bayesian tool for chronology building.  Communications for Statistical Applications and Methods, 25, 2: 131 157.  https://doi.org/10.29220/CSAM.2018.25.2.131
1335 1336 1337 1338 1339	Lentz, D.L., Dunning, N.P., Scarborough, V.L., Magee, K.S., Thompson, K.M., Weaver, E., Carr, C., Terry, R.E., Islebe, G., Tankersley, K.B., Sierra, L.G., Jones, J.G., Buttles, P., Valdez, F., Ramos Hernandez, C.E., 2014. Forests, fields, and the edge of sustainability at the ancient Maya city of Tikal. Proceedings of the National Academy of Sciences of the United States of America 111, 18513–18518. https://doi.org/www.pnas.org/cgi/doi/10.1073/pn
1340 1341	Leyden, B.W., 2002. Pollen evidence for climatic variability and cultural disturbance in the Maya lowlands. Ancient Mesoamerica 13, 85–101. https://doi.org/10.1017/S0956536102131099
1342 1343 1344	Leyden, B.W., Brenner, M., Dahlin, B.H., 1998. Cultural and climatic history of Cobá, a lowland Maya City in Quintana Roo, Mexico. Quaternary Research 49, 111–122. https://doi.org/10.1006/qres.1997.1941
1345 1346	Lindbo, D.L., Stolt, M.H., Vepraskas, M.J., 2010. Redoximorphic features, in: Interpretation of Micromorphological Features of Soils and Regoliths. Elsevier, Amsterdam, pp. 129–147.
1347 1348 1349	Lugo-Hubp, J., Aceves-Quesada, J.F., Espinasa-Pereña, R., 1992. Rasgos geomorfológicos mayores de la Península de Yucatán. Revista Instituto de Geologia. Universidad National Autonoma de Mexico. Instituto de Geologia 10, 143–150.
1350 1351	Lugo-Hubp, J., Garcia, M.T., 1999. El relieve de la Península de Yucatán. In: García de Fuentes, in: Atlas de Procesos Territoriales En Yucatán. Fac. Arq. UADY-PROFESA, México, pp. 155–162.
1352 1353	Lundell, C.L., 1937. The vegetation of the Petén, Carnegie Institution of Washington Publication. ed. Carnegie Institution, Washington.
1354 1355	Macaire, J.J., Bernard, J., Di-Giovanni, C., Hinschberger, F., Limondin-Lozouet, N., Visset, L., 2006.  Quantification and regulation of organic and mineral sedimentation in a late-Holocene

1356	floodplain as a result of climatic and human impacts (Taligny marsh, Parisian Basin, France).
1357	The Holocene 16, 647–660. https://doi.org/10.1191/0959683606hl961rp
1358	Macaire, J.J., Di-Giovanni, C., Hinschberger, F., 2005. Relations entre production organique et apports
1359	terrigènes dans les sediments fluviatiles holocènes : observations et interprétations
1360	hétérodoxes. Comptes Rendus des Geosciences 337, 735–744.
1361	https://doi.org/10.1016/j.crte.2005.03.017
1362	Magaña, V., Amador, J.A., Medina, S., 1999. The Midsummer Drought over Mexico and Central
1363	America. J. Climate 12, 1577–1588. https://doi.org/10.1175/1520-
1364	0442(1999)012<1577:TMDOMA>2.0.CO;2
1365 1366	Marsh, J E., Timoney, K.P., 2005. How long must northern saxicolous lichens be immersed to form a waterbody trimline? Wetlands, The Society of Wetland Scientists 25, 495–499.
1367	Medina-Elizalde, M., Burns, S.J., Lea, D.W., Asmerom, Y., von Gunten, L., Polyak, V., Vuille, M.,
1368	Karmalkar, A., 2010. High resolution stalagmite climate record from the Yucat´an Peninsula
1369	spanning the Maya terminal classic period. Earth Planet. Sci. Lett. 298, 255–262.
1370	https://doi.org/10.1016/j.epsl.2010.08.016
1371	Meybeck, M., 1995. Les lacs et leur bassin, in: Limnologie Générale, Collection d'écologie. Masson,
1372	Paris, pp. 6–59. ISBN 2-225-84687-1.
1373	Meyers, P.A., 1994. Preservation of elemental and isotopic source identification of sedimentary
1374	organic matter. Chemical Geology 114, 289–302. https://doi.org/10.1016/0009-
1375	2541(94)90059-0
1376	Miall, A.D., 2000. Principles of sedimentary basin analysis. (3 <sup>rd</sup> Ed.) Springer-Verlag, Berlin
1377	Heidelberg, pp. 616.
1378	Mueller, A., Islebe, G.A., Hooghiemstra, H., Grzesik, D., Anselmetti, F., Ariztegui, D., Brenner, M.,
1379	Curtis, J.H., Hodell, D.A., Venz, K., 2009. Climate drying and associated forest decline in the
1380	lowlands of northern Guatemala during the late Holocene. Quaternary Research 71, 133-
1381	141. https://doi.org/10.1016/j.yqres.2008.10.002
1382	Nondédéo, P., Castanet, C., Purdue, L., Lemonnier, E., Dussol, L., Hiquet, J., Garnier, A., Testé, M.,
1383	2020a. Archaeological and Paleo-Environmental Reconstructions in the Tropical Maya Area:
1384	The Case of Naachtun (Guatemala), in: Different Times? Archaeological and Environmental
1385	Data from Intra-Site and Off-Site Sequences., Proceedings of the XVIII UISPP World Congress,
1386	Paris. Archaeopress Publishing, pp. 94–110.
1387	Nondédéo, P., Cotom, J., Méndez, J., Olbregts, M., 2020b. Prospección arqueológica en la
1388	microrregión de Naachtun (Operación II.1), in: Proyecto Petén-Norte Naachtun 2019-2022:
1389	Informe de La Décima Temporada de Campo 2019. CNRS/Université de Paris 1/CEMCA.
1390	Informe entregado al Instituto de Antropología e Historia de Guatemala, Guatemala city, pp.
1391	31–96.
1392	Nondédéo, P., Sion, J., Lacadena, A., Cases, I., Hiquet, J., 2021. From Nobles to Kings: the Political and
1393	Historical Context of Naachtun at the End of the Classic Period, in: Maya Kingship: Rupture or

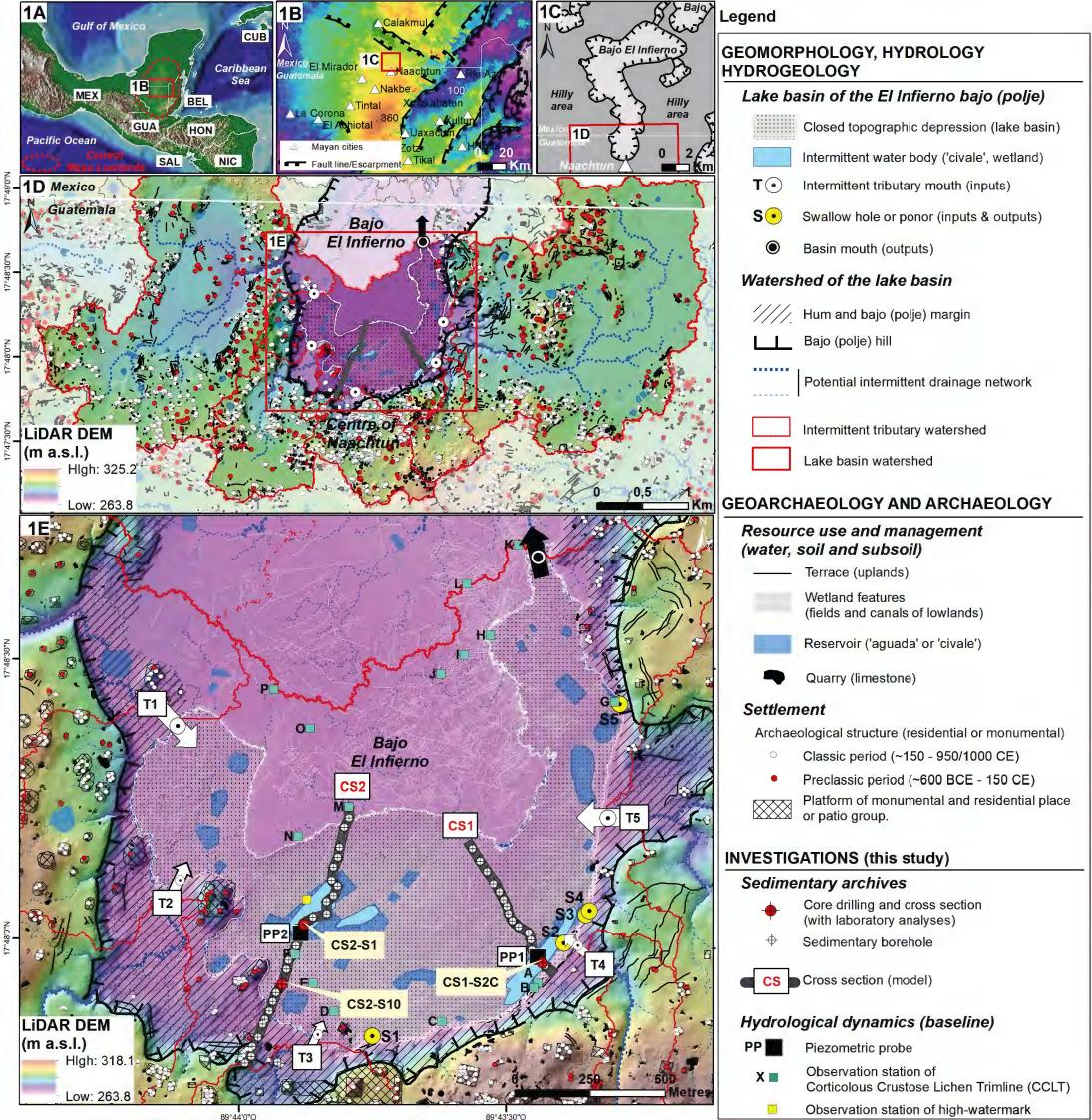
1394 1395	Gainesville.
1396 1397 1398	Nondédéo, P., Lacadena, A., Cases, J.I., 2019. Teotihuacanos y Mayas en la 'Entrada' de 11 EB' (378 d.C.): nuevos datos de Naachtun, Petén, Guatemala. Rev. Esp. Antropol. Amer 49, 53–75. https://doi.org/10.5209/reaa.64960
1399 1400 1401 1402	Nondédéo, P., Lemonnier, E., Hiquet, J., Purdue, L., Castanet, C., Dussol, L., In press. Shaping an agrarian Maya town: settlement pattern and land use dynamics at Naachtun, in: The Flexible Maya City: Attraction, Contraction, and Planning in Lowland Urban Dynamics. University Press of Colorado.
1403 1404	O'Leary, M.H., 1981. Carbon isotope fractionation in plants. Phytochemistry 20, 553–567. https://doi.org/10.1016/0031-9422(81)85134-5
1405 1406	O'Leary, M.H., 1988. Carbon isotopes in photosynthesis. Bioscience, 38: 328-336. https://doi.org/10.2307/1310735
1407 1408 1409	Padilla, R., 2007. Evolución geológica del sureste mexicano desde el Mesozoico al presente en el contexto regional del Golfo de México. Bol. Soc. Geol. Mex. 59, 19–42. https://doi.org/10.18268/bsgm2007v59n1a3
1410 1411 1412 1413	Padrón, R.S., Gudmundsson, L., Decharme, B., Ducharne, A., Lawrence, D.M., Jiafu, M., Peano, D., Krinner, G., Kim, H., Seneviratne, I., 2020. Observed changes in dry-season water availability attributed to human-induced climate change. Nat. Geosci. 13, 477–481. https://doiorg.inee.bib.cnrs.fr/10.1038/s41561-020-0594-1
1414 1415 1416 1417	Palerm, A., Wolf, E.R., 1957. Ecological potential and cultural development in Mesoamerica, in: Studies in Human Ecology: A Series of Lectures given at the Anthropological Society of Washinton., Pan-American Union Social Science Monographs. Pan-American Union, Washington, pp. 1–38.
1418 1419 1420	Patiño, A., 2013. Pottery, Differentiation, Integration, and Politics: Ceramic Consumption and Manufacture in Naachtun during the Preclassic and the Early Classic Periods. University of Calgary, Calgary.
1421 1422 1423 1424	Perla-Barrera, D., Sion, J., 2018. Operación IV.1: Análisis cerámico de la Temporada 2018, in: Proyecto Petén-Norte Naachtun 2015-2018: Informe de La Novena Temporada de Campo 2018, CNRS/Université de Paris 1/CEMCA. Informe Entregado al Instituto de Antropología e Historia de Guatemala. pp. 137–162.
1425 1426 1427 1428	Perla-Barrera, D., Sion, J., 2017. Operación IV.1: Análisis cerámico de la Temporada 2017, in: Proyecto Petén-Norte Naachtun 2015-2018: Informe de La Octava Temporada de Campo 2017, CNRS/Université de Paris 1/CEMCA. Informe Entregado al Instituto de Antropología e Historia de Guatemala. pp. 215–244.
1429 1430 1431	Perry, E., Payton, A., Pederson, B., Velazquez-Oliman, B., 2009. Groundwater geochemistry of the Yucatan Peninsula, Mexico, constraints on stratigraphy and hydrogeology. J. Hydrol. 367, 27–40. https://doi.org/10.1016/j.jhydrol.2008.12.026

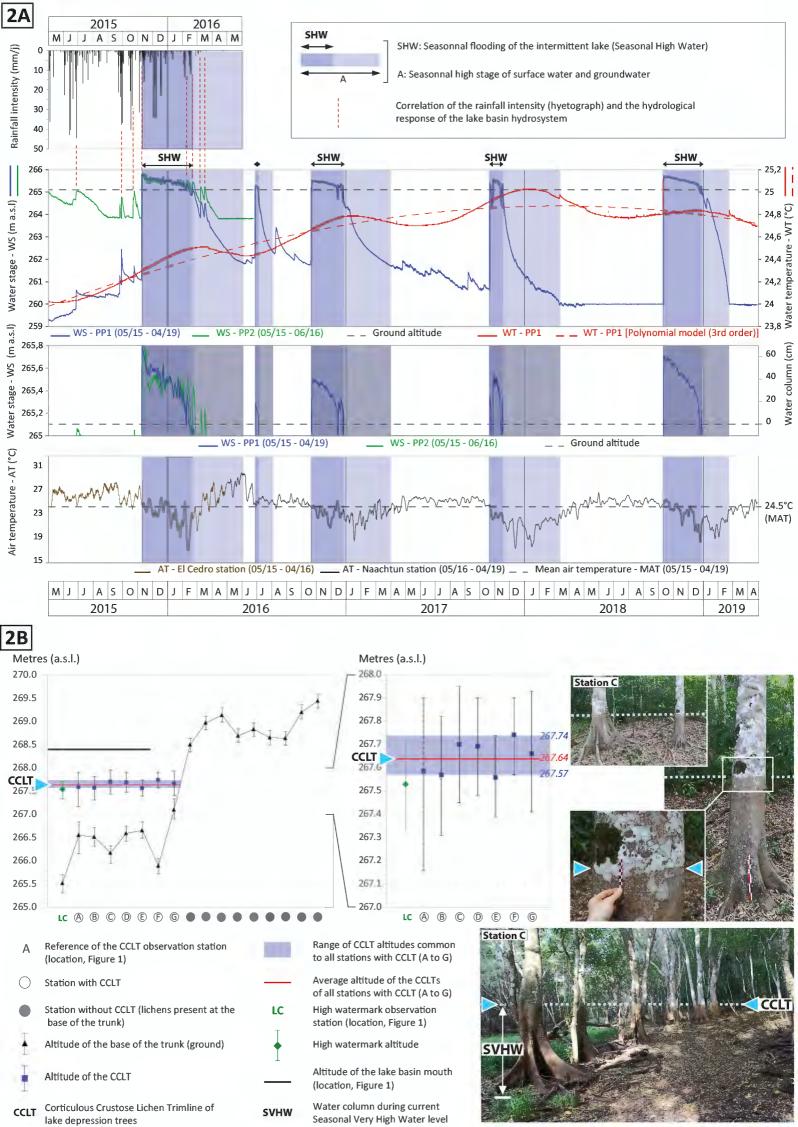
1432	Perry, E.C., Velazquez-Oliman, G., Leal-Bautista, R.M., Dunning, N.P., 2019. The Icaiche Formation:
1433	Major contributor to the stratigraphy, hydrogeochemistry and geomorphology of the
1434	northern Yucatán Peninsula, Mexico. BOL. SOC. GEOL. MEX. 71, 741 – 760.
1435	http://dx.doi.org/10.18268/BSGM2019v71n3a7
1436	Pohl, M.D., Pope, K.O., Jones, J.G., Jacob, J.S., Piperno, D.R., deFrance, S.D., Lentz, D.L., Gifford, J.A.,
1437	Danforth, M.E., Josserand, J.K., 1996. Early agriculture in the Maya lowlands. Latin American
1438	Antiquity 7, 355–372. https://doi.org/10.2307/972264
1439	Pope, K.O., Dahlin, B.H., 1993. Radar detection and ecology of ancient Maya canal systems: Reply to
1440	Adams et al. Journal of Field Archaeology 20, 379–383. https://doi.org/10.2307/530065
1441	Pope, K.O., Dahlin, B.H., 1989. Ancient Maya wetland agriculture: new insights from ecological and
1442	remote sensing research. Journal of Field Archaeology 87–106.
1443	https://doi.org/10.2307/529883
1444	Qin, B., Yang, L., Chen, F., Zhu, G., Zhang, L., Chen, Y., 2006. Mechanism and control of lake
1445	eutrophication. Chinese Sci Bull 51, 2401–2412. https://doi.org/10.1007/s11434-006-2096-y
1446	Ravbar N., Mayaud C., Blatnik M., Petrič M., 2021. Determination of inundation areas within karst
1447	poljes and intermittent lakes for the purposes of ephemeral flood mapping. Hydrogeology
1448	Journal 29, 213–228, https://doi.org/10.1007/s10040-020-02268-x
1449	Reimer P. et al., 2020. The IntCal20 Northern Hemisphere radiocarbon age calibration curve (0–55 cal
1450	kBP). Radiocarbon 62, 725–757. https://doi.org/10.1017/RDC.2020.41
1451	Ricketson, O.G., Jr., 1937. Uaxactun, Guatemala, Group E - 1926–1931. Part 1: The excavations.,
1452	Carnegie Institution of Washington Publication. ed. Carnegie Institution, Washington.
1453	Robert, C., Casella, G., 2004, Monte Carlo Statistical Methods. Springer-Verlag New York, pp 649.
1454	https://doi.org/10.1007/978-1-4757-4145-2
1455	Roberts, P., Hunt, C., Arroyo-Kalin, M., Evans, D., Boivin, N., 2017. The deep human prehistory of
1456	global tropical forests and its relevance for modern conservation. Nature Plants 3.
1457	https://doi.org/10.1038/nplants.2017.93
1458	Rosenmeier, M.F., Brenner, M., Hodell, D.A., Martin, J.B., Curtis, J.H., Binford, M.W., 2016. A model
1459	of the 4000-year paleohydrology (δ18O) record from Lake Salpetén, Guatemala. Global and
1460	Planetary Change 138, 43–55. https://doi.org/10.1016/j.gloplacha.2015.07.006
1461	Rosenmeier, M.F., Hodell, D.A., Brenner, M., Curtis, J.H., Guilderson, T.P., 2002a. A 4000 year
1462	lacustrine record of environmental change in the southern Maya lowlands, Petén,
1463	Guatemala. Quat. Res. 57, 183–190. https://doi.org/10.1006/qres.2001.2305
1464	Rosenmeier, M.F., Hodell, D.A., Brenner, M., Curtis, J.H., Martin, J.B., Anselmetti, F., Ariztegui, D.,
1465	Guilderson, T.P., 2002b. Influence of vegetation change on watershed hydrology: implications
1466	for paleoclimatic interpretation of lacustrine $\delta 180$ records. J. Paleolimnol. 27, 117–131.
1/167	https://doi.org/10.1023/A:1013535930777

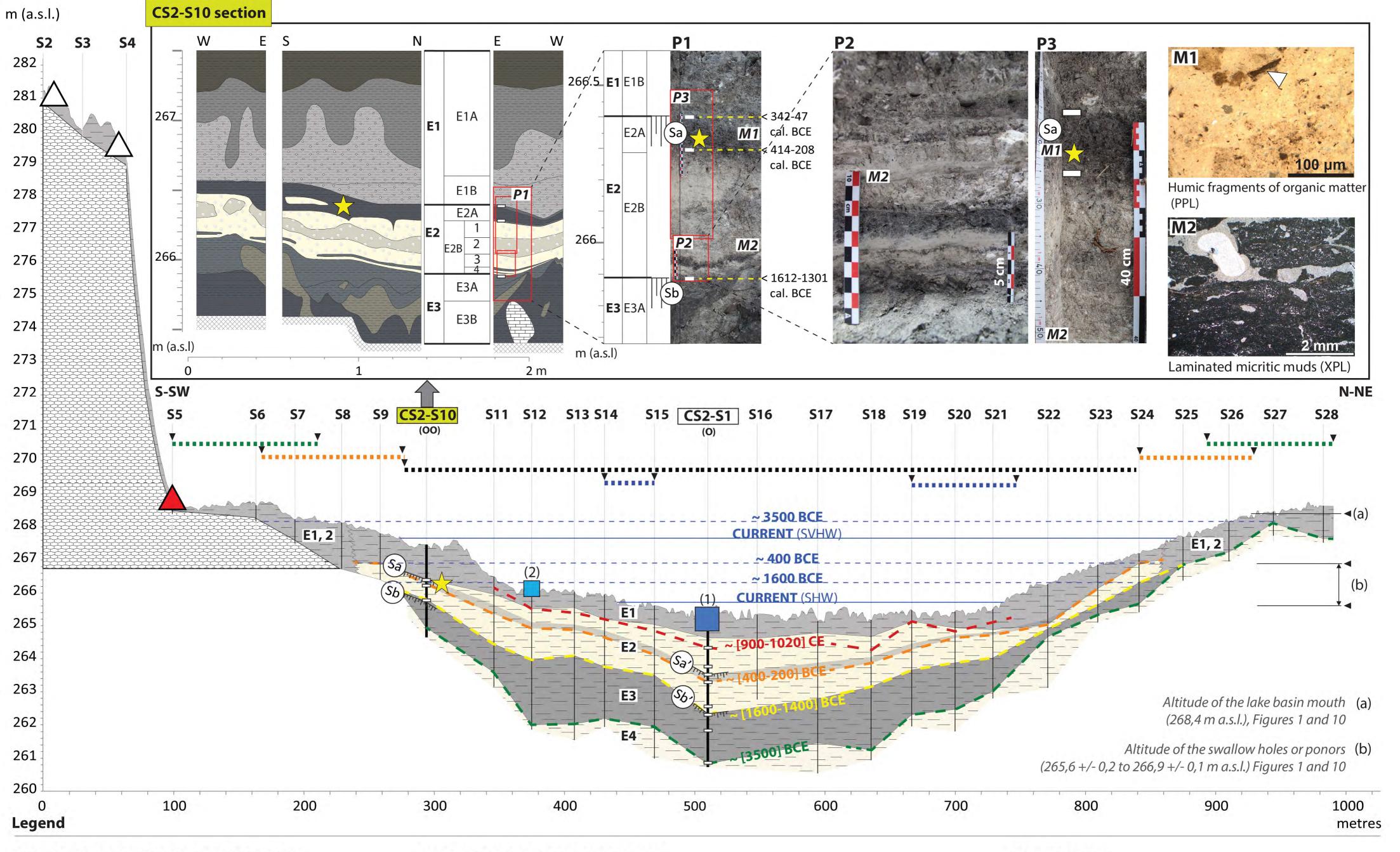
1468 1469 1470	Symposium on Ecology and Management of Riparian Shrub Communities, General Technical Report INT-289. Forest Service, USDA, Ogden, UT, pp. 18–24.
1471 1472	Salomon, J.N., 2006. Précis de karstologie, 2ème édition revue et corrigée. ed, Scieteren. Presses Universitaires de Bordeaux, Pessac.
1473 1474 1475 1476	Schröder, T., van't Hoff, J, Lopez-Saez, J.A., Viehberg, F.V., Melles, M., Reicherter, K., 2018. Holocene climatic and environmental evolution on the southwestern Iberian Peninsula: A high-resolution multi-proxy study from Lake Medina (Cadiz, SW Spain), Quaternary Science Reviews 198, 208-225 https://doi.org/10.1016/j.quascirev.2018.08.030
1477 1478	Servicio Geológico Mexicano, S., 2007. Carta Geológico-Minera, Estados de Campeche, Quintana Roo, y Yucatán.
1479 1480	Siemens, A., 1978. Karst and the pre-Hispanic Maya in the Southern Lowlands, in: Pre-Hispanic Maya Agriculture. University of New Mexico Press, Albuquerque, pp. 117–144.
1481 1482 1483	Simmons, C.S., Tarano, T., Pinto, Z., 1959. Clasificación de reconocimiento de los suelos de la República de Guatemala, Instituto de Agropecuario Nacional, Servicio Cooperativa Inter-Americana de Agricultura. ed. Guatemala City.
1484 1485	Small, R.J.O., de Szoeke, S.P., Xie, S.P., 2007. The Central American midsummer drought: Regional aspects and large-scale forcing. J. Climate 20, 4853–4873. https://doi.org/10.1175/JCLI4261.1
1486 1487	Stephens, L. et al., 2019. Archaeological assessment reveals Earth's early transformation through land use. Science 365, 897–902. https://doi.org/10.1126/science.aax1192
1488 1489	Stoops, J., Vepraskas, M.J., 2003. Guidelines for Analysis and Description of Soil and Regolith Thin Sections, Soil Science Society of America. ed.
1490 1491	Talbot, M.R., Allen, P.A., 1996. Lakes, in: Sedimentary Environments: Processes, Facies and Stratigraphy. Blackwell Science Ltd, pp. 83–124.
1492 1493 1494	Taylor, M.A., Enfield, D.B., Chen, A.A., 2002. Influence of the tropical Atlantic versus the tropical Pacific on Caribbean rainfall. Journal of Geophysical Research 107, 3127. https://doi.org/doi:10.1029/2001JC001097
1495 1496 1497	Taylor, M.A., Stephenson, T.S., Owino, A., Chen, A.A., Campbell, J.D., 2011. Tropical gradient influences on Caribbean rainfall. Journal of Geophysical Research 116, 14 pp. https://doi.org/10.1029/2010JD015580
1498 1499 1500	Testé, M., 2020. Histoire Naturelle des Phytolithes des Basses Terres Mayas. Implications pour la reconstitution des Paléoenvironnements et des interactions sociétés-environnements. (Unpublished Ph.D thesis). Université de Paris 1 Panthéon-Sorbonne, Paris.
1501 1502 1503	Testé, M., Garnier, A., Limondin-Lozouet, N., Oxlaj, E., Castanet, C., Purdue, L., Lemonnier, E., Dussol, L., Nondédéo, P., 2020. The phytoliths of Naachtun (Petén, Guatemala): Development of a Modern Reference for the Characterization of Plant Communities in the Maya Tropical

1504 1505	https://doi.org/10.1016/j.revpalbo.2019.104130
1506 1507 1508	Timoney, K.P., Marsh, J., E., 2004. Lichen Trimlines in Northern Alberta: Establishment, Growth Rates and Historic Water Levels. The Bryologist 107, 429–440. https://doi.org/10.1639/0007-2745(2004)107[429:LTINAE]2.0.CO;2
1509 1510 1511	Turner, B.L., Harrison, P.D., 1983. Pulltrouser Swamp and Maya raised fields: A summation, in: Pulltrouser Swamp: Ancient Maya Habitat, Agriculture, and Settlement in Northern Belize. University of Texas Press, Austin, pp. 246–269.
1512 1513 1514	Turner, B.L., Sabloff, J.A., 2012. Classic period collapse of the central Maya lowlands: Insights about human-environment relationships for sustainability. Proc. Natl. Acad. Sci. U.S.A. 109, 13908–13914. https://doi.org/10.1073/pnas.1210106109
1515 1516	Veldkamp, E., Schmidt, M., Powers, J.S., 2020. Deforestation and reforestation impacts on soils in the tropics. Nat Rev Earth Environ. https://doi.org/10.1038/s43017-020-0091-5
1517 1518 1519	Verrecchia, E.P., 2002. Géodynamique du carbonate de calcium à la surface des continents, in Miskovsky JC. (ed) Géologie de La Préhistoire. Géopré, Presses Universitaires de Perpignan, Paris, pp. 233–258.
1520 1521 1522	Vinson, G.L., 1962. Upper Cretaceous and Tertiary stratigraphy of Guatemala. Bulletin of the American Association of Petroleum Geologists 46, 425–456. https://doi.org/10.1306/BC743835-16BE-11D7-8645000102C1865D
1523 1524	Wahl, D., Byrne, R., Anderson, L., 2014. An 8700 year paleoclimate reconstruction from the southern Maya lowlands. Quat. Sci. Rev. 103, 19–25. https://doi.org/10.1016/j.quascirev.2014.08.004
1525 1526 1527	Wahl, D., Byrne, R., Schreiner, T., Hansen, R., 2006. Holocene vegetation change in the northern Peten and its implications for Maya prehistory. Quaternary Research 65, 380–389. https://doi.org/10.1016/j.yqres.2005.10.004
1528 1529 1530	Wahl, D., Byrne, R., Schreiner, T., Hansen, R.D., 2007. Palaeolimnological evidence of late-Holocene settlement and abandonment in the Mirador Basin, Peten, Guatemala. Holocene 17, 813–820. https://doi.org/10.1177/0959683607080522
1531 1532 1533 1534	Wahl, D., Estrada-Belli, F., Anderson, L., 2013. A 3400 year paleolimnological record of prehispanic human-environment interactions in the Holmul region of the southern Maya lowlands. Palaeogeography, Palaeoclimatology, Palaeoecology 379–380, 17–31. https://doi.org/10.1016/j.palaeo.2013.03.006
1535 1536 1537 1538	Wahl, D., Hansen, R., Byrne, R., Anderson, L., 2016. Holocene climate variability and anthropogenic impacts from Lago Paixban, a perennial wetland in Petén, Guatemala. Special issue on climate change and archaeology in Mesoamerica. Glob. Planet. Chang. 138, 70–81. https://doi.org/10.1016/j.gloplacha.2015.09.011

1539 1540 1541	Walker, Debra S., Kathryn Reese-Taylor y Peter Mathews, 2006. Después de la caída: Una redefinición del Clásico Temprano Maya, in XIX Simposio de Investigaciones Arqueológicas en Guatemala, Museo Nacional de Arqueología y Etnología, Guatemala, pp.715-728.
1542	Webb, E.A., Schwarcz, H.P., Healy, P.F., 2004. Detection of ancient maize in lowland Maya soils using
1543	stable isotope isotopes: evidence from Caracol, Belize. Journal of Archaeological Science 31,
1544	1039–1052. https://doi.org/10.1016/j.jas.2004.01.001
1545	Wirth, S.B., Gilli, A., Niemann, H., Dahl, T.W., Ravasi, D., Sax, N., Hamann, Y., Peduzzi, R., Peduzzi, S.,
1546	Tonolla, M., Lehmann, M.F., Anselmetti, F.S., 2013. Combining sedimentological, trace metal
1547	(Mn, Mo) and molecular evidence for reconstructing past water-column redox conditions:
1548	The example of meromictic Lake Cadagno (Swiss Alps), Geochimica et Cosmochimica Acta,
1549	120, 220–238 http://dx.doi.org/10.1016/j.gca.2013.06.017
1550	Xu, H., Liu, B., Wu, F., 2010. Spatial and temporal variations of Rb/Sr ratios of the bulk surface
1551	sediments in Lake Qinghai. Geochemical Transactions 11. https://doi.org/10.1186/1467-
1552	4866-11-3
1553	Zeng, Y., Chen, J., Zhu, Z., Li, J., Wang, J., Wan, G., 2012. The wet Little Ice Age recorded by sediments
1554	in Huguangyan Lake, tropical South China. Quat. Int. 263, 55-62.
1555	https://doi.org/10.1016/j.quaint.2011.12.022







# LITHOLOGY, PEDOLOGY, STRATIGRAPHY

Weakly carbonated silty clay

Carbonated clayey silt and carbonate tufa

Mollusk shells and calcified alguae

Limestone (bedrock)

Palaeosol (Sa: cultivated soil)

**Ex** Main sediment body

**Exx** Main sediment zone (Figures 6 and 7)

## Field works (this study)

गागा(Sx)

**SX** Sediment borehole

Core drilling (O) or cross section (OO) with sedimentological and geochemical analyses (Figures 6 and 7)

# **HYDROLOGY, PALAEOHYDROLOGY**

# **Water stages**

CURRENT Altitude for SHW or SVHW [measurements (1) and (2)]

~[X] BCE/CE Minimum altitude for SHW [estimations (3)]

# **Shoreline zones**

Current [measurements (1)]

From 200 BCE to 1000 CE [estimations (3), (\*) (\*\*)]

~ 400 BCE [estimations (3), (\*)] ~ 3500 BCE [estimations (3),(\*)] (\*) Minimum altitude for SHW

(\*\*) Shoreline fluctuation zone during the period

# Field works (this study)

Measurements (piezometric probes): period 2015-2019 (Figure 2A). Regime of seasonal high water level (SHW)(265.7 +/- 0.1 m a.s.l.)

(2) Estimations (lichen trimline and the high watermark): occurences between 2000 and 2015 (Figure 2B). Regime of seasonal very high water level (SVHW) (267,64 +/- 0.1 m a.s.l.)

(3) Palaeohydrological interpretations (Figures 10 and 11)

# CHRONOLOGY

□ Chronological marker (¹⁴C date) (Table 1)

~ [X] BCE/CE

Isochronous line, palaeotopographic profile
 and palaeobathymetric line for the specified age (deduced from the morphostratigraphy, the lithofacies and the chronological markers)

## **ARCHAEOLOGY**

 $\triangle$ 

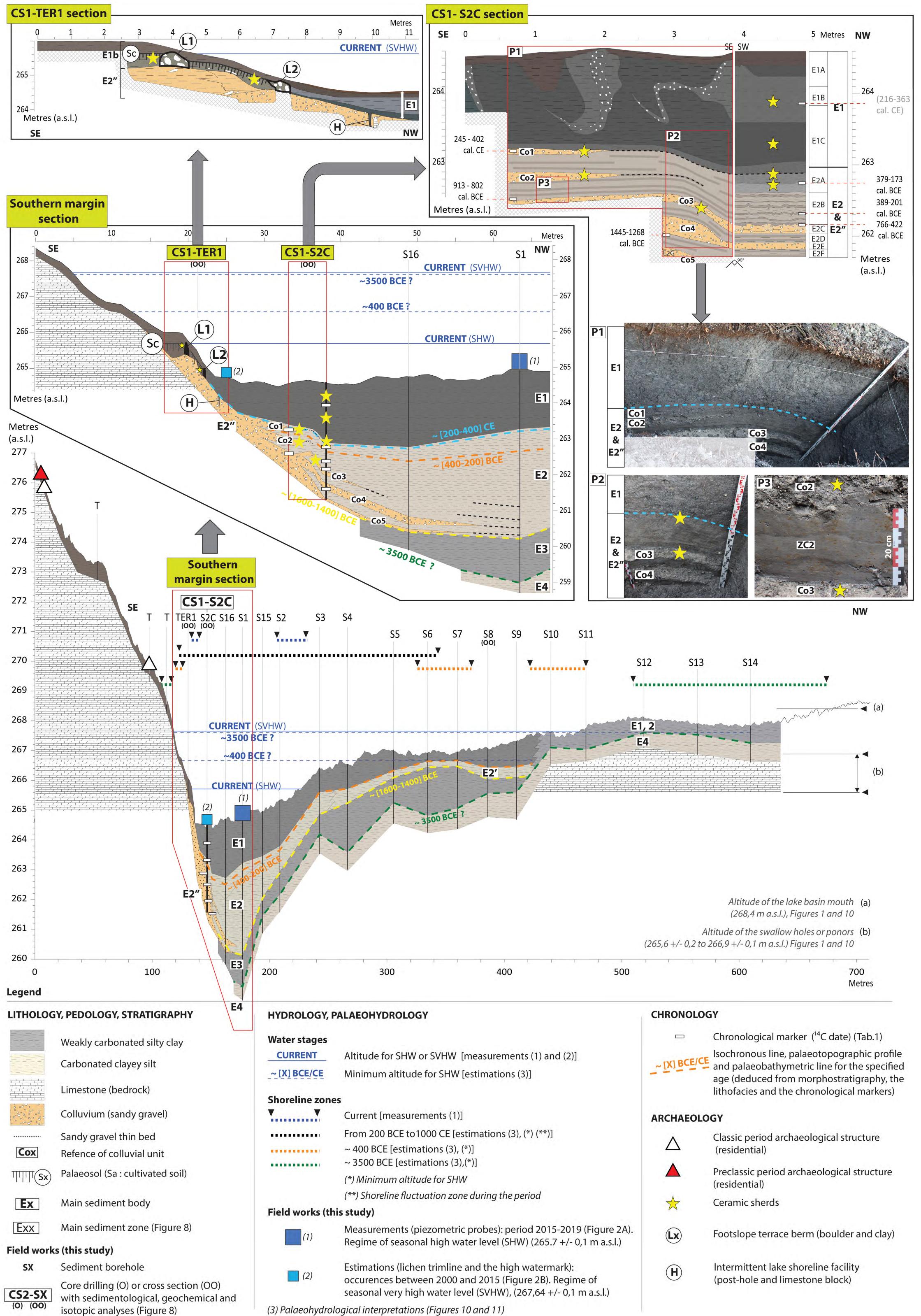
Classic period archaeological structure (residential)

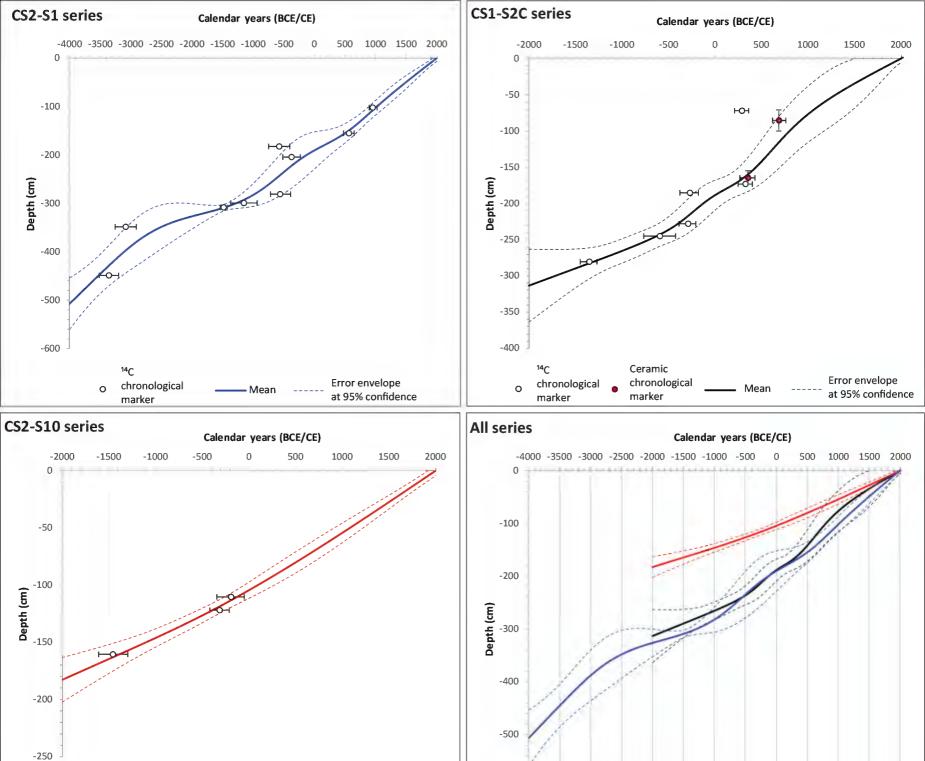


Preclassic period archaeological structure (residential)



Ceramic sherds





-600

CS2-S1

CS1-S2C

CS2-S10

Error envelope

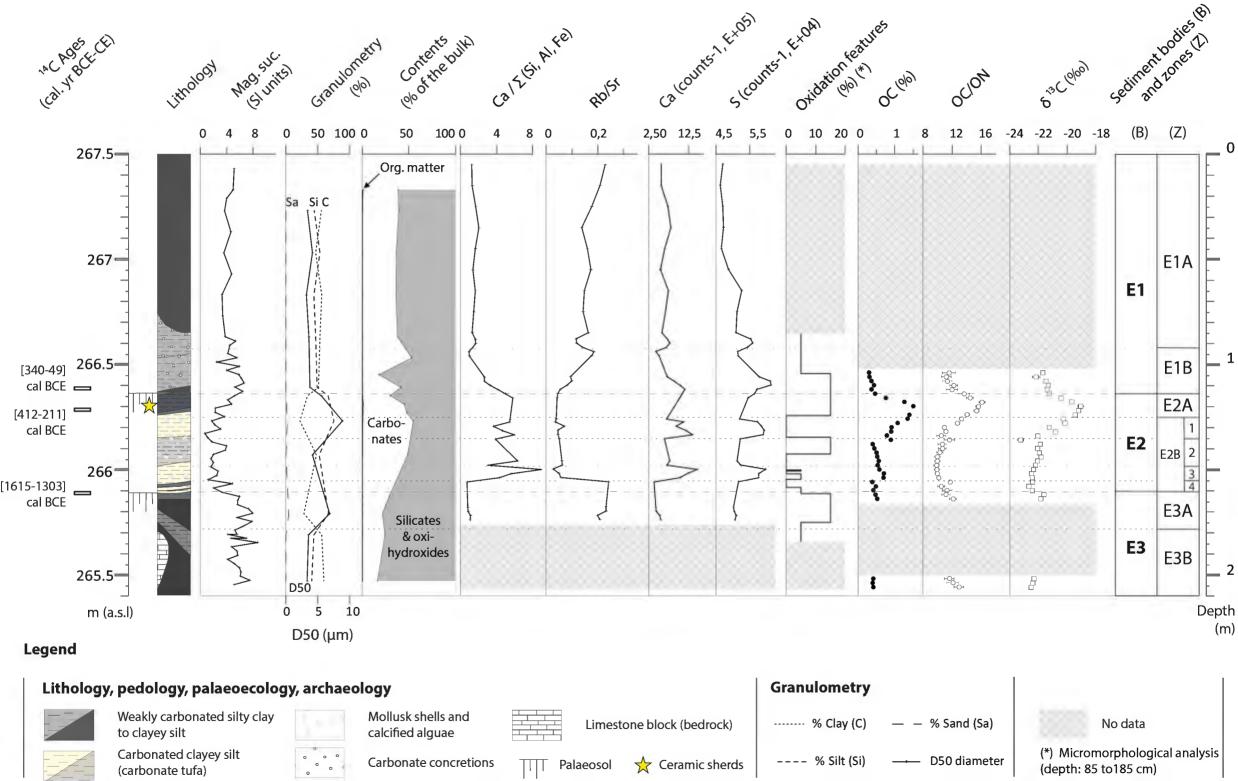
at 95% confidence

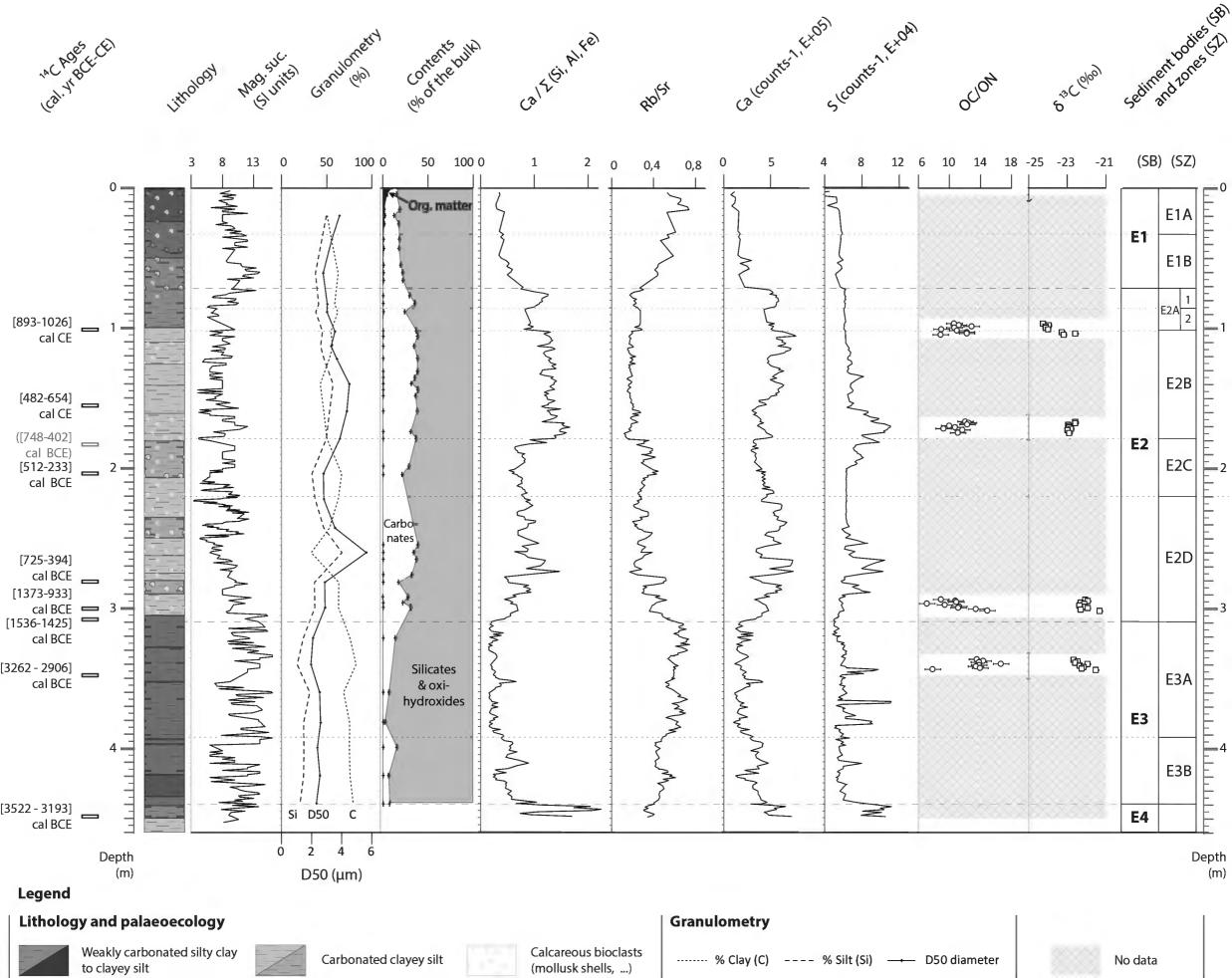
14C

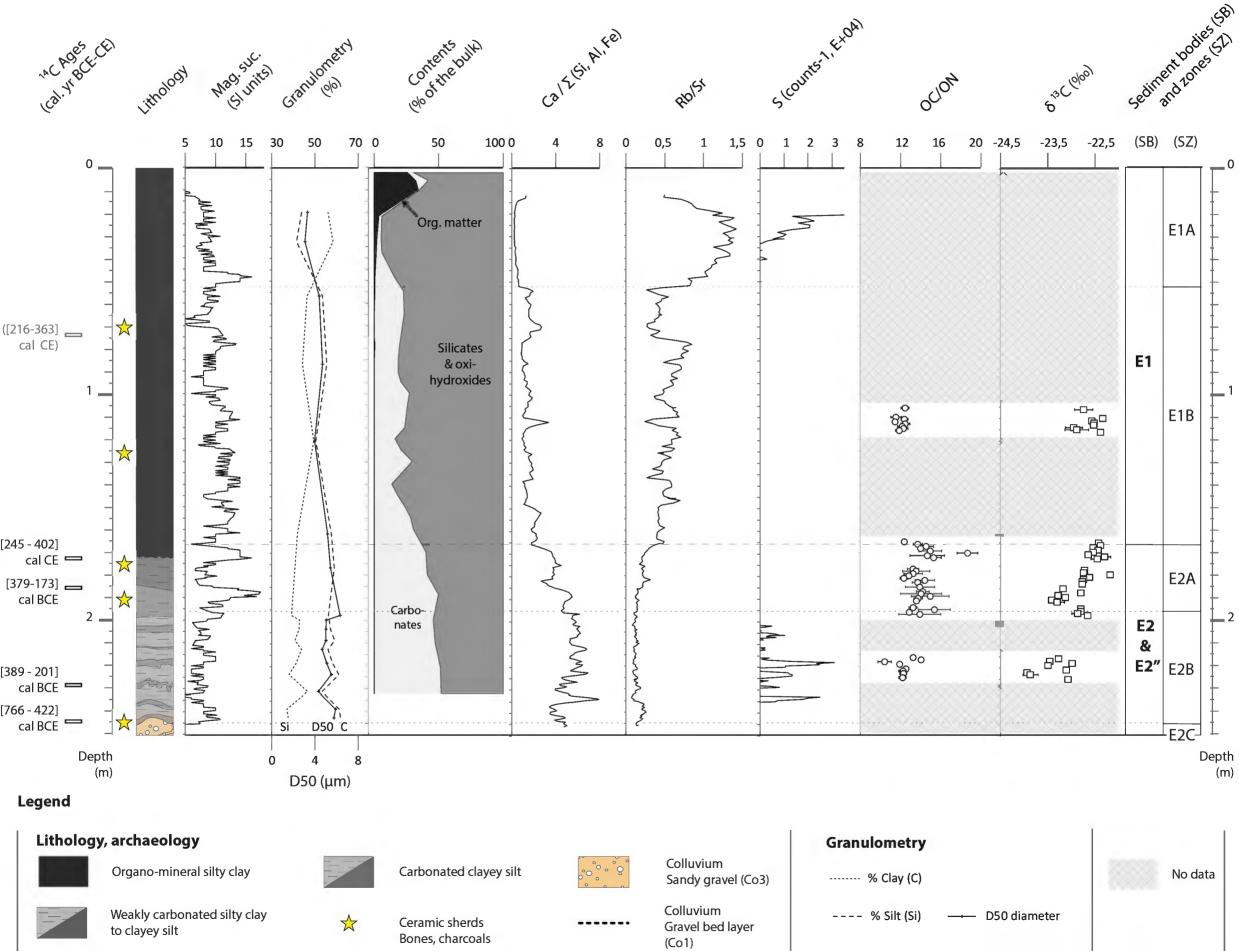
chronological

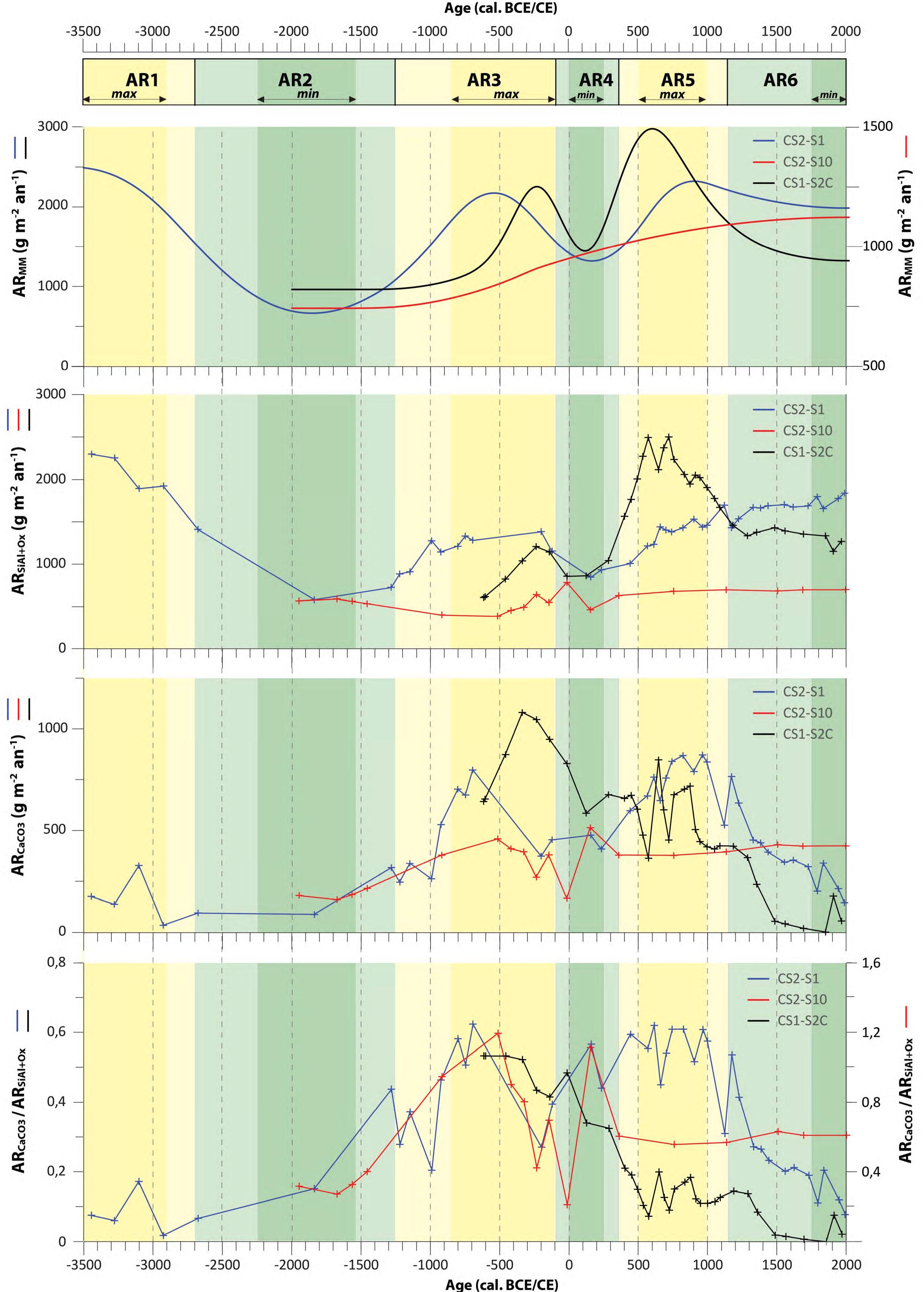
marker

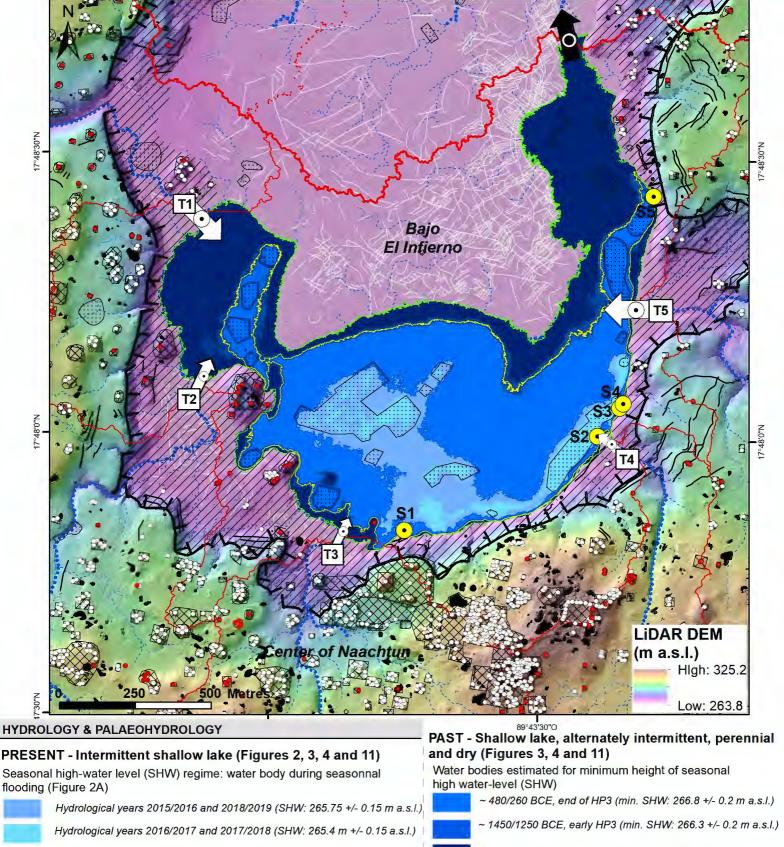
Mean











Seasonal very high-water level (SVHW) regime: perimetre of water body during seasonnal flooding (Figure 2B)



Hydrological year(s) between 2000/2001 and 2015/2016 (Water-level: 267.64 +/- 0.15 m a.s.l.)



Closed topographic depression (perimeter of the lake basin)





Hum and bajo (polje) margin



Potential intermittent drainage network



Intermittent tributarie watershed



Lake basin watershed

Bajo (polje) hill



Intermittent tributary mouth (inputs)



Swallow hole or ponor (inputs & outputs) Basin mouth (outputs)

~3500 BCE, end of HP1 (min. SHW: 268.2 +/- 0.2 m a.s.l.)

Between ~ 480/260 BCE and the Present (HP4 to HP7), minimum heights of SHW were lower than during ~ 480/260 BCE.

### RESOURCE USE AND MANAGEMENT (WATER, SOIL, SUBSOIL)

Reservoir ('aguada' or 'cival')



Wetland features (fields and canals of lowlands)

Terrace (uplands)

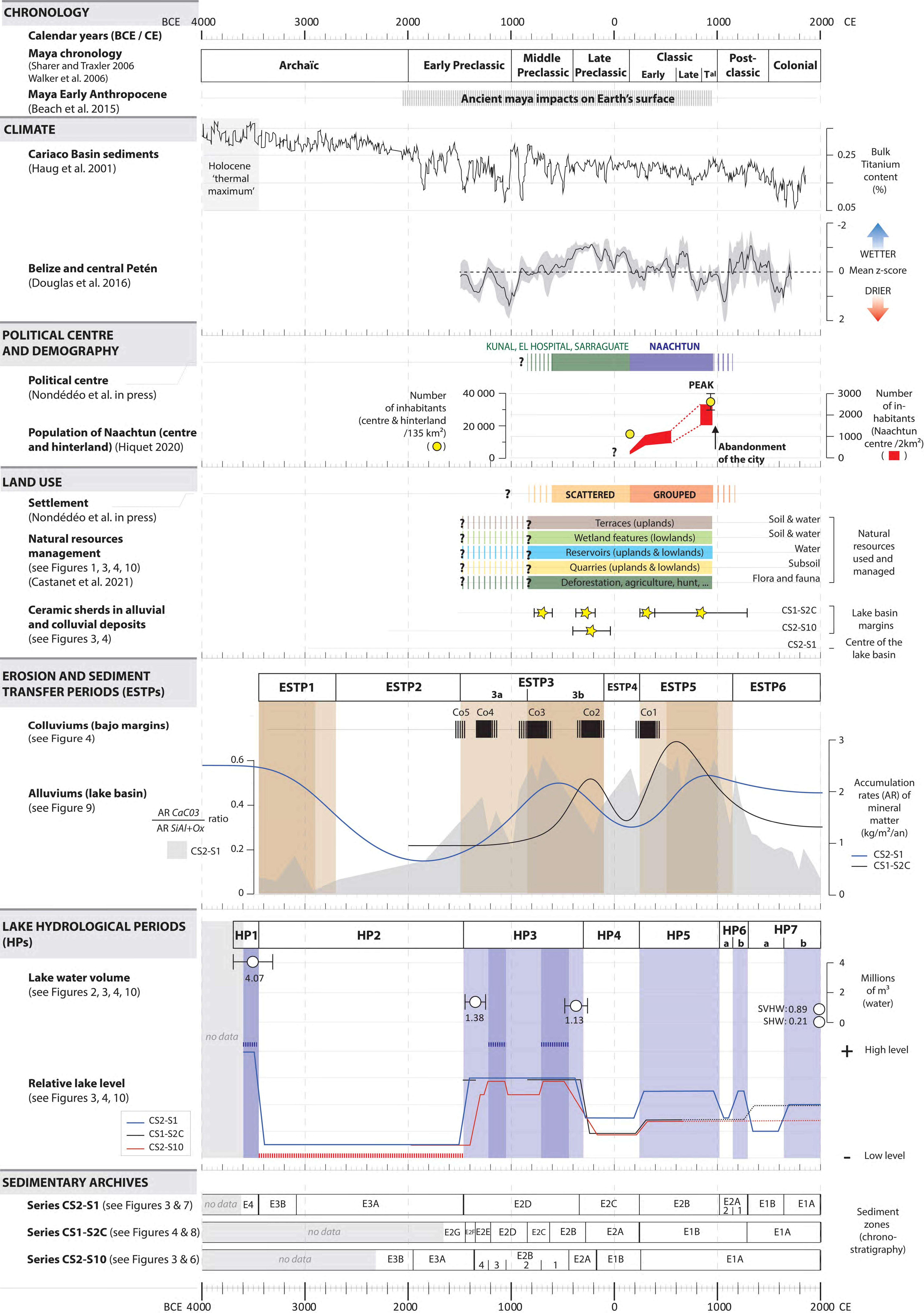


Quarry

## SETTLEMENT

Archaeological structure (residential or monumental)

- Classic period (~150 950/1000 CE)
- Preclassic period (~600 BCE 150 CE)
- Platform of monumental and residential place



Sample code	Laboratory code	Series	Zone	Depth m b.s.	Material	<sup>14</sup> C age yr BP	Age yr BCE-CE
NA15 BA M2 S10-3	Poz-75416	CS2_S10	E1B	110-111	Organic sediment	2115 ± 30	[ BCE 342: BCE 323] 4.4% [ BCE 201: BCE 47] 91.1%
NA15 BA M2 S10-4	Poz-75251	CS2_S10	E2A	121-122	Organic sediment	2305 ± 35	[ BCE 414: BCE 351] 66.4% [ BCE 302: BCE 208] 29.1%
NA15 BA M2 S10-11	Poz-75252	CS2_S10	E3A	160-161	Organic sediment	3190 ± 60	[ BCE 1612: BCE 1374] 87.9% [ BCE 1351: BCE 1301] 7.6%
NA13 M2 S1 n1	Poz-68787	CS2_S1	E2B	101-101.5	Organic sediment	1070 ± 30	[ CE 893: CE 929] 23.6% [ CE 944: CE 1026] 71.8%
NA M2 S1 n2	Poz-68448	CS2_S1	E2B	154-157	Organic sediment	1480 ± 40	[ CE 482: CE 492] 1% [ CE 536: CE 654] 94.5%
NA13 M2 S1 C4b-32	Beta - 474443	CS2_S1	E2C	182-183	Organic sediment	2420 ± 30	[ BCE 748: BCE 688] 13.9% [ BCE 666: BCE 642] 5.9% [ BCE 567: BCE 402] 75.6%
NA13 S1 C5-4	Beta - 474444	CS2_S1	E2C	204-205	Organic sediment	2330 ± 30	[ BCE 512: BCE 508] 0.2% [ BCE 481: BCE 358] 91.4% [ BCE 278: BCE 258] 2.4% [ BCE 246: BCE 233] 1.4%
NA13 M2 S1 C6-29	Beta - 474445	CS2_S1	E2D	280-281	Organic sediment	2390 ± 30	[ BCE 725: BCE 706] 3% [ BCE 664: BCE 651] 2.1% [ BCE 545: BCE 394] 90.4%
NA M2 S1 1	Poz-134072	CS2_S1	E2D	299-300	Charcoal (charcoal layer)	2930 ± 60	[ BCE 1373 : BCE 1354] 1,4% [ BCE 1298 : BCE 973] 92,4% [ BCE 955 : BCE 933] 1,7%
NA M2 S1 n3	Poz-68450	CS2_S1	E3A	307-309	Organic sediment	3225 ± 30	[ BCE 1536: BCE 1425] 95.4%
NA M2 S1 n4	Poz-68728	CS2_S1	E3A	348-349	Organic sediment	4385 ± 35	[ BCE 3262: BCE 3251] 1% [ BCE 3100: BCE 2906] 94.5%
NA M2 S1 n5	Poz-68729	CS2_S1	E4	448-449	Organic sediment	4620 ± 40	[ BCE 3522: BCE 3336] 93.7% [ BCE 3211: BCE 3193] 1.7%
NA13 M1 S2C n1	Poz-68786	CS1-S2C	E1B	71-73	Organic sediment	(1775 ± 30)	([ CE 216: CE 363] 95.4%)
NA13 USD-1	Poz-90901	CS1-S2C	Co1	140-141	Charcoal (charcoal layer)	1740 ± 30	[ CE 245: CE 402] 95.4%
NA13 M1 S2C-n2b	Poz-70741	CS1-S2C	E2A	185-186.5	Organic sediment	2205 ± 35	[ BCE 379: BCE 173] 95.4%
NA13 M1 S2C-n3b	Poz-70742	CS1-S2C	E2B	208-210	Organic sediment	2700 ± 35	[ BCE 913: BCE 803] 95.4%
NA M1 S2c n4	Poz-68451	CS1-S2C	E2B	227-229	Organic sediment	2235 ± 30	[ BCE 389: BCE 342] 24.2% [ BCE 321: BCE 201] 71.2%
NA M1 S2c n5	Poz-68727	CS1-S2C	E2B	245-246	Organic sediment	2470 ± 30	[ BCE 766: BCE 465] 93.4% [ BCE 436: BCE 422] 2.1%
NA13 M1 S2C-n6b	Poz-70743	CS1-S2C	E2F	232-233	Organic sediment	3105 ± 35	[ BCE 1445: BCE 1268] 95.4%